Monthly Notices
of the
ROYAL ASTRONOMICAL SOCIETY

Mon. Not. R. Astron. Soc. **417,** 2721–2736 (2011) doi:10.1111/j.1365-2966.2011.19439.x

# The role of secular evolution in the black hole growth of narrow-line Seyfert 1 galaxies

G. Orban de Xivry,[1⋆] R. Davies,[1] M. Schartmann,[1,2] S. Komossa,[1,3,4,5] A. Marconi,[6] E. Hicks,[7] H. Engel[1] and L. Tacconi[1]

[1]*Max Planck Institut für extraterrestrische Physik, Giessenbachstrasse, D-85748 Garching, Germany*
[2]*Universitäts-Sternwarte München, Scheinerstrasse 1, D-81679 München, Germany*
[3]*Technische Universität München, Fakultät für Physik, James-Franck-Strasse, D-85748 Garching, Germany*
[4]*Excellence Cluster Universe, TUM, Boltzmannstrasse 2, D-85748 Garching, Germany*
[5]*Max Planck Institut für Plasmaphysik, Boltzmannstrasse 2, D-85748 Garching, Germany*
[6]*Dipartimento di Fisica e Astronomia, Universitá degli Studi di Firenze, Largo E. Fermi 2, 50125 Firenze, Italy*
[7]*Department of Astronomy, University of Washington, Box 351580, Seattle, WA 98195, USA*

Accepted 2011 July 12. Received 2011 July 12; in original form 2011 April 21

**ABSTRACT**

Narrow-line Seyfert 1 (NLS1) galaxies show extreme properties with respect to the other Seyfert galaxies. Indeed, they are thought to be accreting at Eddington rates and to possess low-mass black holes. Therefore, they may represent a key class of objects for understanding the co-evolution of black holes and their host galaxies. We propose that NLS1s represent a class of active galactic nucleus in which the black hole growth is, and has always been, dominated by secular evolution. First, by looking at the NLS1 host galaxy properties in the literature, we show that the evolution of NLS1s is presently driven by secular processes, much more so than for broad-line Seyfert 1s (BLS1s). Secondly, we study the bulges of NLS1 and BLS1 galaxies. Our results demonstrate that NLS1 host bulges are pseudo-bulges and are statistically different from BLS1 bulges. This difference points to the particular importance of secular processes in the past evolution of their hosts. We build on this result to understand the implications on their evolution and the duration of their duty cycle. We show that NLS1s are not necessarily in a special phase of black hole growth and that several Gyr are required for their black hole masses to become similar to BLS1s. Finally, in the light of our results, we discuss the location of NLS1 galaxies on the $M_{\rm BH}$–$\sigma$ plane and speculate about the connection between the NLS1 galaxy properties and their black hole spin.

**Key words:** galaxies: active – galaxies: bulges – galaxies: evolution – galaxies: Seyfert.

## 1 INTRODUCTION

Since their discovery, narrow-line Seyfert 1 (NLS1) galaxies have always been recognized as particular objects holding important clues on the driving mechanisms of nuclear activity. First identified as objects similar to Seyfert 1s with narrower Balmer lines, they were soon recognized as having exceptional spectral properties, both in their emission lines and in their continuum (see Komossa 2008, for a review). In fact, as shown through principal components analysis (e.g. Boroson 2002), NLS1 galaxies are mostly clustered at one extreme end of the active galactic nucleus (AGN) parameter space (strongest Fe II/[O III] emission and lowest luminosity). Likewise, they are thought to possess small mass black holes (BHs) and to have high Eddington accretion rates. In this sense, NLS1s could represent key objects in understanding the AGN phenomena and the co-evolution of massive BHs and their host galaxies.

While the main defining criteria of NLS1s with respect to broad-line Seyfert 1 (BLS1) galaxies is the empirical threshold at full width at half-maximum (FWHM)(H$\beta$) $\sim 2000\,{\rm km\,s^{-1}}$, the properties of NLS1s have been extensively studied across many wavelength ranges. Trends and correlations have been identified using first small samples and later corroborated by larger surveys (e.g. Véron-Cetty & Véron 2001; Williams, Pogge & Mathur 2002; Zhou et al. 2006). Many scenarios have been considered to explain these properties, in particular their high accretion rates ($L/L_{\rm Edd} \simeq 1$; e.g. Boroson 2002; Grupe 2004, and reference therein) and low BH masses (typically of order $10^6\,{\rm M}_\odot$; e.g. Boller, Brandt & Fink 1996; Zhou et al. 2006; Ryan et al. 2007), but also e.g. outflows, winds and density effects, high metallicity, particular broad-line region (BLR) thicknesses and densities, etc. (see Komossa 2008, and references therein). While these scenarios can elucidate the nuclear

⋆E-mail: xivry@mpe.mpg.de

properties of NLS1s, they hardly explain the origin of the fundamental differences between NLS1s and BLS1s and, in particular, that NLS1s appear to be more than just Seyfert 1s with narrow lines. A few key questions could be formulated as follows: which particular mechanisms would lead to the Eddington accretion rates commonly seen in NLS1s but observed less often in BLS1s? What causes the difference in BH growth of NLS1s and BLS1s that results in low-mass BHs in the former case? Could differing host galaxy evolution explain the differences between NLS1 and BLS1 galaxies?

In this paper, rather than studying the active nuclei, we investigate the host galaxies of NLS1s and contrast their properties to those of BLS1s, pursuing the hypothesis that different host galaxy evolution could explain the differences between NLS1s and BLS1s. In particular, we explore the relative role of secular processes in the evolution of NLS1 and BLS1 galaxies. Reviewing the literature on the morphology and the star formation in NLS1 and BLS1 hosts, we emphasize, in Section 2, the present-day differences in their respective host galaxies. Afterwards, in Section 3, we turn to the past evolution of NLS1 and BLS1 hosts. We perform a bulge–disc decomposition of samples of NLS1 and BLS1 galaxies and look at their bulge properties. Using previously established criteria (Kormendy & Kennicutt 2004; Fisher & Drory 2008; Gadotti 2009), we are able to distinguish pseudo- from classical bulges. This enables us to determine the main processes that have driven the evolution of the NLS1 and BLS1 hosts. We analyse the differences of NLS1 and BLS1 host bulge property distributions, concluding that NLS1 galaxies contain pseudo-bulges and, hence, have always been dominated by secular evolution. Finally, in Sections 4 and 5, we investigate the cosmological context of the NLS1 host phenomenon driven by such an evolutionary mode. We then note the link between secular evolution and rapidly spinning BHs, and speculate on the location of NLS1 galaxies on the $M_{\rm BH}$–$\sigma$ relation. We conclude by summarizing our picture of the NLS1 galaxy phenomenon and present ways to further test our proposition.

When calculating distances and look-back times, we assume a general relativistic Friedmann–Robertson–Walker (FRW) cosmology with matter density parameter $\Omega_{\rm m} = 0.3$, vacuum energy density parameter $\Omega_\Lambda = 0.7$ and Hubble parameter $H_0 = 70\,{\rm km\,s^{-1}\,Mpc^{-1}}$.

## 2 SECULAR EVOLUTION IN NLS1 HOST GALAXIES

In this section, we review the literature that has been published concerning the differences in the host galaxy properties of NLS1s and BLS1s. We focus in particular on the morphology and the star formation rate, and emphasize the role of present secular processes in distinguishing between these two classes of type 1 AGN.

### 2.1 Morphological properties

#### *2.1.1 Large-scale bars*

The morphology of NLS1 host galaxies has been studied in several papers (Crenshaw, Kraemer & Gabel 2003; Deo, Crenshaw & Kraemer 2006; Ohta et al. 2007; Ryan et al. 2007). The main results can be summarized as follows:

*NLS1 host galaxies are likely to be strongly barred (much more than BLS1 ones) and their nuclear dust morphology is likely to be a grand-design spiral.*

The bar frequency among NLS1 and BLS1 host galaxies has been studied by Crenshaw et al. (2003) and Ohta et al. (2007). The first

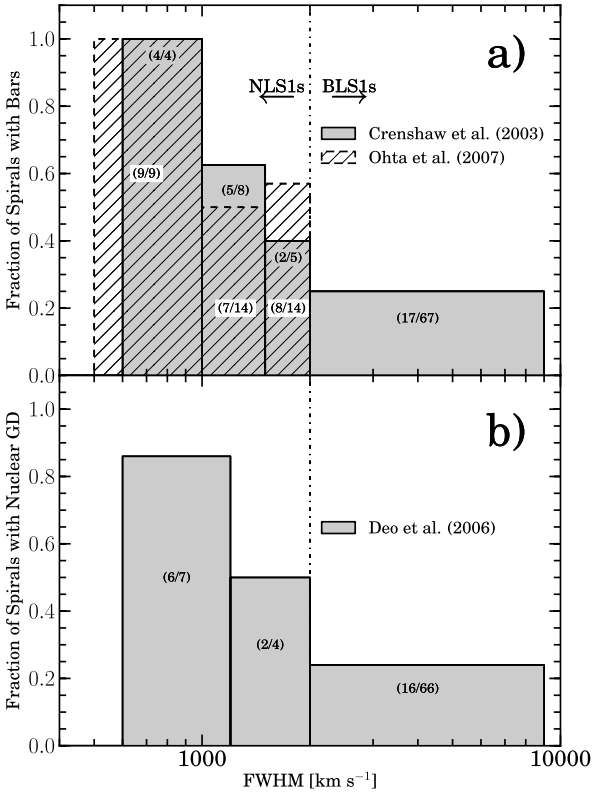


**Figure 1.** Histograms presenting the fraction of Seyfert 1 spirals (a) with bars and (b) with nuclear grand-design spirals as a function of the FWHM of their broad emission line, H$\beta$. Drawn from data reported in Crenshaw et al. (2003), Ohta et al. (2007) and Deo et al. (2006).

paper reports a visual study based on a *Hubble Space Telescope* (*HST*) survey of 91 Seyfert galaxies (13 NLS1s and 78 BLS1s) at $z \leq 0.035$ (Malkan, Gorjian & Tam 1998) and six additional NLS1s at $z \leq 0.084$ (*HST* archives in the Véron-Cetty, Véron & Gonçalves 2001 sample). The results are striking: 91 per cent of the sample is classified as spiral galaxies among which 65 per cent of NLS1s have bars, and 25 per cent of BLS1s have bars. More particularly, the authors look at the fraction of barred spiral galaxies in their sample as a function of the FWHM of the broad component of the H$\beta$ emission line. As presented in Fig. 1, they obtain a clear difference between the two regimes of NLS1s and BLS1s. We note that in this figure, since FWHM measurements are not available for every BLS1, we have made a single bin for the BLS1 class.

The results from Ohta et al. (2007) are more conservative. They use a heterogeneous set of data of NLS1 galaxies and look at the morphology and the possible trends with the NLS1 properties. They perform a visual and a quantitative classification based on ellipse fitting of isophotes. While they confirm the high bar fraction among (spiral) NLS1 hosts, they do not observe a clear trend with the FWHM. Nevertheless, if we consider only the fraction of spirals with strong bars (SB but not SAB), the trend does appear clearly using their visual classification (as represented in Fig. 1). Turning to their quantitative classification, we note that one of the criteria Ohta et al. use to identify the bars is an ellipticity $\epsilon_{\rm bar} \geq 0.25$, where $\epsilon_{\rm bar} = \max(\epsilon_{\rm galaxy})$. However, a common practice to identify *strong* bars is to use $\epsilon_{\rm bar} \geq 0.45$ (e.g. Shlosman, Peletier & Knapen 2000). Applying this latter criterion on their sample by examining the ellipse fit plots, we obtain, for the respective bins in Fig. 1 (i.e. 500–1000, 1000–1500 and 1500–2000 km s$^{-1}$), bar fractions (i.e.

89, 46 and 57 per cent) similar to their visual classification (i.e. 100, 50 and 57 per cent, see Fig. 1).

#### *2.1.2 Circumnuclear morphology*

In a study of nuclear dust morphology in a matched-paired sample of active/inactive galaxies and barred/unbarred galaxies, Martini et al. (2003) show that grand-design nuclear dust spirals are only found in galaxies with a large-scale bar. However, while not finding any universal nuclear morphology in active galaxies, they do find similar features in the circumnuclear environments of both active and inactive galaxies. In another study, Deo et al. (2006) investigate the nuclear dust morphology in NLS1 and BLS1 host galaxies based only on the *HST* survey conducted by Malkan et al. (1998). Their study also shows that the grand-design nuclear dust spirals are largely present in barred galaxies. They classify the nuclear structures and find that (1) the nuclear dust morphologies in NLS1/BLS1, barred/unbarred are mainly nuclear dust spirals, (2) in the 'nuclear dust spiral' class, NLS1s are more likely to have grand-design spirals than BLS1s. Fig. 1 also shows that this fraction of grand-design spirals in NLS1s follows the same trend with the FWHM(H$\beta$) as the bar fraction.

As we expect strong bars to drive a circumnuclear spiral structure (Maciejewski 2004a,b) and to drive gas inwards (Sakamoto et al. 1999; Sheth et al. 2005), we expect the presence of such asymmetries in host galaxies to result in an enhanced star formation in the central kiloparsecs.

### 2.2 Star formation

In a recent paper, Sani et al. (2010) study the link between star formation in the central kiloparsecs versus FWHM(H$\beta$) in NLS1 and BLS1 host galaxies. After discussing carefully possible luminosity and distance effects, they conclude that NLS1s are associated with more intense star formation than BLS1s (with on average a star formation to AGN ratio >two times larger in NLS1s). More generally, they find that type 1 AGN with narrower broad emission lines reside in hosts containing more intense star-forming regions.

Finally, they find a connection between high Eddington ratio and high star formation rates concluding that NLS1s are characterized by smaller BH mass, larger Eddington ratio and stronger star formation activity compared to their broad-line counterparts.

### 2.3 Secular processes all the way to the SMBH

As discussed above, the current morphology of NLS1 host galaxies is distinguishable from other Seyfert galaxies. Indeed, in contrast to BLS1s, NLS1 galaxies are likely to be strongly barred and to show more intense central star formation. This is in line with the fact that bars are known to drive gas into the central kiloparsecs (Sakamoto et al. 1999; Sheth et al. 2005), and that nuclear star formation is enhanced in barred galaxies (Ho et al. 1997).

While no universal fuelling mechanism for low-luminosity AGN seems to operate in galactic nuclei (Martini et al. 2003), the NLS1 host morphology typically exhibits a circumnuclear grand-design spiral. This appears to be linked to the presence of strong bars (Martini et al. 2003; Deo et al. 2006), and indeed bars are able to drive circumnuclear spiral structures (Maciejewski 2004a,b). Hence, NLS1 galaxies show uninterrupted asymmetries able to drive the gas inwards from a few kpc to a few tens of pc. The particular strength of secular processes in NLS1s could therefore account for the high central star formation and presumably to the large Eddington rates observed in NLS1s.

## 3 BULGES OF NLS1 HOST GALAXIES

Since strong secular evolution is currently occurring in NLS1s, it is important to ask whether or not secular processes have shaped the NLS1 host galaxies by dominating their past evolution and hence influencing their BH growth.

We address this issue by examining the bulges of NLS1 host galaxies and comparing them to those of BLS1s, since one can expect to observe evolutionary-dependent bulge characteristics. Specifically, an evolution driven mainly by galaxy mergers will result in different bulge properties than if the evolution is mainly driven by internal secular evolution.

In this section, we compare NLS1 and BLS1 galaxies by performing a photometric bulge–disc decomposition of homogeneous samples of NLS1s and BLS1s. This comparison is put in perspective with previous studies on the distinction between pseudo- and classical bulges in inactive galaxies (Kormendy & Kennicutt 2004; Fisher & Drory 2008; Gadotti 2009), and also on the bulge–disc decomposition of two galaxy samples composed exclusively of NLS1s (Ryan et al. 2007; Mathur et al. 2011).

### 3.1 Pseudo-bulges and secular evolution in disc galaxies

Kormendy & Kennicutt (2004) review in detail the formation of pseudo-bulges by secular processes. As dense central components of galaxies, pseudo-bulges differ from classical bulges in that they were made slowly by discs out of disc material while classical bulges are 'merger-built' bulges. Therefore, pseudo-bulges are formed by internal secular processes such as bar instabilities, spiral structures, etc. as opposed to galaxy mergers or external secular evolution (minor mergers, prolonged gas infall, etc.).

As pseudo-bulges retain memory of their discy origin, it is possible to disentangle them from classical bulges. Kormendy & Kennicutt (2004) pointed out the Sérsic index as one way to identify them. Indeed, since a pseudo-bulge forms from gas accreting from the disc, it has a surface brightness profile similar to that of the outer disc and therefore would have a low Sérsic index $n_{\rm b} \sim 1$–2.

Fisher & Drory (2008) have studied in great detail the structure of classical bulges and pseudo-bulges using high-resolution data (77 inactive galaxies with data in the *HST* archive and $z \lesssim 0.01$). They use morphological signatures to first visually classify the bulges of nearby galaxies as pseudo or classical. They then perform a bulge–disc decomposition and study in particular the distribution of Sérsic indices. They find that, statistically, pseudo-bulges have Sérsic indices $n_{\rm b} < 2$ while classical bulges have $n_{\rm b} > 2$. This result shows that the Sérsic index is a good statistical tool to test if a class of objects has classical or pseudo-bulges.

Finally, Gadotti (2009) also study pseudo- and classical bulges using a large, low-resolution, Sloan Digital Sky Survey (SDSS) sample of galaxies ($\sim$1000 inactive galaxies with $0.02 \leq z \leq 0.07$). He uses the position in the $\langle\mu_{\rm e}\rangle$–$r_{\rm e}$ plane, also called the Kormendy relation,[1] to study the bulge properties and identifies pseudo-bulges as being fainter in surface brightness for a given half-light radius

[1] Relation between the mean effective surface brightness within the effective radius $\langle\mu_{\rm e}\rangle$ and the half-light radius $r_{\rm e}$, which is a projection of the photometric Fundamental Plane.

(much fainter than predicted by the correlation fit to elliptical galaxies). Where Gadotti (2009) clearly sees independent groups in his *i*-band density plot of the Kormendy relation ($\langle\mu_e\rangle$–$r_e$ relation), Fisher & Drory (2008, 2010) only find that pseudo-bulges scatter around the photometric projections of the Fundamental Plane.

Nevertheless, all these authors (Fisher & Drory 2008, 2010; Gadotti 2009) agree that most of the pseudo-bulges have a low Sérsic index $n_b < 2$ and that they tend to be less prominent than classical bulges (in particular, they tend to have a low bulge-to-total light ratio).

Based on these considerations for bulge classification in inactive galaxies, we will use the Sérsic index to identify the prevailing bulge type in the NLS1 and BLS1 populations as pseudo or classical. We will then study the prominence of NLS1 and BLS1 bulges.

### 3.2 Bulge–disc decomposition

Building on the work of Fisher & Drory (2008) for inactive galaxies, we select archive *HST* images of Seyfert galaxies to study the bulges of active galaxies, in order to assess whether the bulge characteristics of NLS1s and BLS1s might explain, by their evolutionary implications, the distinctions between these two classes of AGN. Crucially, by performing the bulge–disc decomposition for samples of both NLS1s and BLS1s, we minimize the impact of any systematic errors that our fitting procedure might generate.

We select NLS1 and BLS1 galaxies from the Malkan et al. (1998) *HST* imaging survey of nearby AGN. This survey contains a uniform sample of 91 Seyfert 1 galaxies at $z \leq 0.035$ observed with the Wide Field Planetary Camera 2 (WFPC2) through the *F606W* filter. This sample, also used by Crenshaw et al. (2003) and Deo et al. (2006) in their morphological studies, contains 11 NLS1 galaxies and 80 BLS1 galaxies. The 11 NLS1 galaxies are genuine NLS1s as identified by Véron-Cetty et al. (2001) on the basis of their optical spectra (broad component of H$\beta$ $< 2000\,\mathrm{km\,s^{-1}}$ and strong Fe II emission) and are listed in the catalogue of Véron-Cetty & Véron (2010). We therefore initially select all the 11 NLS1 galaxies available, as well as 21 of the 80 BLS1s. The BLS1 sample selection is made in a way to roughly match the ∼25 per cent fraction of such hosts that are strongly barred (Crenshaw et al. 2003). Their individual Seyfert classifications are reported in Table 1. These are taken from Véron-Cetty & Véron (2010) with two exceptions. IC 1816 is classified by Márquez et al. (2004) as a type 1. Because their spectrum shows clear evidence of broad emission, we have adopted this classification. For NGC 5252, we have followed the classification as a type 1.9 given in Osterbrock & Martel (1993), because the presence of broad H$\alpha$, with a measured FWHM of $\sim$2500 km s$^{-1}$, is confirmed by Acosta-Pulido et al. (1996). We note that the broad H$\alpha$ is very clear in polarized light (Tran 2010), and shows dramatic variations over a period of several years. This may be why there is some uncertainty about its classification as a type 1 or 2. Following this initial selection, we refine our sample based on the limited field of view (FoV) of WFPC2 by rejecting objects with $z < 0.010$ or scales $\leq$0.23 kpc arcsec$^{-1}$ in order to obtain a reasonable minimum FoV of $\gtrsim 8 \times 8\,\mathrm{kpc}^2$ on each object. This criterion ensures that the disc of the host can be fitted properly, while the redshift limit of the original source catalogue ensures that the bulge is sufficiently well resolved. The two final samples for which we performed the bulge–disc decomposition are composed of 10 NLS1s and 19 BLS1s, and are given in Table 1. Finally, we check that the mean redshift is not strongly biased with respect to the NLS1 sample ($\langle z_{\mathrm{NLS1}}\rangle = 0.024$, $\langle z_{\mathrm{BLS1}}\rangle = 0.027$), and that no particular circumnuclear morphology has been selected.

To perform the bulge–disc decomposition of these 29 galaxies, we use the two-dimensional profile fitting algorithm GALFIT[2] (Peng et al. 2010). For each galaxy we iteratively fit three components: a Gaussian profile, a Sérsic profile and an exponential profile (see also Appendix A). These components are aimed at modelling, respectively, the nuclei, the bulges and the discs of our galaxies. While these *HST* data of nearby AGN have small pixel scales (see column 6 in Table 1) enabling us to better constrain the central regions of the galaxies, the FoV of WFPC2 ($\sim 35 \times 35\,\mathrm{arcsec}^2$) is small relative to the full extent of the galaxies. This makes it hard to constrain the sky level. This issue has already been addressed to some extent by the refinement of our sample selection to objects with $z \geq 0.010$. We cover it further in Appendix B when we discuss our treatment of the possible coupling between the background level and the exponential profile. Finally, we analyse the robustness of our fit by studying the effect of saturated regions in the images and the dependence of the fits to the point spread function (PSF). We detail our iterative fit procedure in Appendix B, our treatment of additional structures such as bars, rings and spirals, and the particular attention given to the background level. We give also eight examples of our fits in Figs B2 and B3.

The relevant results of our fits are given in Table 2. Among them, the reduced chi-square value $\chi^2_\nu$ from the fit, first indicator of its quality. Our mean $\chi^2_\nu$ values are 1.1 for NLS1s and 1.06 for BLS1s, reflecting the overall acceptability of the fits.

During this process, we have found two objects for which no acceptable bulge– disc decomposition could be performed. Specifically, the morphology of MRK 335 is mainly point like and is better described by a single high Sérsic index profile, while ESO 438G9 seems to be a bulgeless galaxy also consistent with its morphological type. We have therefore excluded these two objects from the bulge analysis discussed in Section 3.3, which is performed on nine NLS1 and 18 BLS1 galaxies.

### 3.3 Structural properties of NLS1 and BLS1 host galaxies

#### *3.3.1 The Sérsic index $n_b$ in the bulges*

In Fig. 2, we compare the results obtained for the nine NLS1 galaxies to the distribution found by Fisher & Drory (2008) for pseudo- and classical bulges. According to their results, the mean Sérsic index of pseudo-bulges is 1.69 with only ∼10 per cent of them having an index greater than 2. For our NLS1 sample, we find $\langle n_b\rangle \sim 1.48$ (and a standard deviation for the distribution of $\sigma_n \sim 0.39$) with none of them significantly exceeding a Sérsic index of 2.

The bottom panel of Fig. 2 compares the distribution of NLS1 and BLS1 host bulge Sérsic indices from the analysis of our samples. While the two distributions are clearly different, BLS1 host bulges also tend to have lower Sérsic indices than the Fisher & Drory (2008) classical bulges. We find $\langle n_b\rangle \sim 2.54$, $\sigma_n \sim 0.97$ for BLS1 host bulges, in contrast to $\langle n_b\rangle \sim 3.49$ obtained by Fisher & Drory for classical bulges. Thus, our results suggest that BLS1s do not have 'pure' classical bulges, but rather mixed bulges composed of pseudo- and classical components.

It is appropriate to mention here the work of Laurikainen et al. (2007). They found that, for inactive galaxies, the mean bulge Sérsic index is ∼2.5 or less across the Hubble sequence. These results can also be interpreted as the existence of a large range of composite bulges between the two extreme 'pseudo-' and 'classical' bulge

[2] http://users.obs.carnegiescience.edu/peng/work/galfit/galfit.html

**Table 1.** *HST* sample of NLS1s and BLS1s. Columns – (1): object name; (2)–(4): J2000 coordinates and redshift from NASA/IPAC Extragalactic Database (NED); (5): luminosity distance in Mpc for an $H_0 = 70\,\mathrm{km\,s^{-1}\,Mpc^{-1}}$, $\Omega_\mathrm{m} = 0.3$ and $\Omega_\Lambda = 0.7$ cosmology; (6): respective scale, the WFPC2 pixel scale is 0.0456 arcsec; (7): morphological classification (from Malkan et al. 1998, MGT); (8) Seyfert classification according to the Véron-Cetty & Véron (2010) catalogue except for IC 1816 and NGC 5252, see also the main text; S1 classification designates a type 1 AGN with unspecified subtype; (9): FWHM of the broad component of H$\beta$ (or in a few cases, H$\alpha$), the NLS1 measurements are from Véron-Cetty et al. (2001), the BLS1 measurements are taken from Crenshaw et al. (2003), see also references therein.

| Object name | RA (J2000) | Dec. (J2000) | $z$ | $D$ (Mpc) | Pixel scale (kpc arcsec$^{-1}$) | Morpho. (MGT) | AGN type | FWHM (km s$^{-1}$) |
|---|---|---|---|---|---|---|---|---|
| (1) | (2) | (3) | (4) | (5) | (6) | (7) | (8) | (9) |
| NLS1 sample | | | | | | | | |
| KUG 1136 | 11 39 13.9 | +33 55 51 | 0.032 | 131.84 | 0.64 | SB0 | S1n | 1145 |
| MRK 0042 | 11 53 41.8 | +46 12 43 | 0.024 | 99.83 | 0.48 | SBa | S1n | 865 |
| MRK 0335[a] | 00 06 19.5 | +20 12 11 | 0.025 | 109.12 | 0.50 | ? | S1n | 1350 |
| MRK 0359 | 01 27 32.5 | +19 10 44 | 0.017 | 71.31 | 0.35 | SBb/c | S1n | 900 |
| MRK 0382 | 07 55 25.3 | +39 11 10 | 0.034 | 139.74 | 0.68 | SBa | S1n | 1280 |
| MRK 0493 | 15 59 09.6 | +35 01 47 | 0.031 | 127.87 | 0.62 | S(B)a | S1n | 740 |
| MRK 0766 | 12 18 26.5 | +29 48 47 | 0.012 | 50.65 | 0.25 | SBc | S1n | 1630 |
| MRK 0896 | 20 46 20.8 | −02 48 45 | 0.027 | 111.91 | 0.54 | Sc | S1n | 1135 |
| MRK 1044 | 02 30 05.5 | −08 59 53 | 0.016 | 67.20 | 0.33 | Sa | S1n | 1010 |
| NGC 4748 | 12 52 12.4 | −13 24 53 | 0.014 | 58.94 | 0.29 | Sa | S1n | 1565 |
| BLS1 sample | | | | | | | | |
| ESO 438G9[b] | 11 10 48.0 | −28 30 04 | 0.024 | 99.83 | 0.48 | SBc/d | S1 | 5000 |
| F1146 | 08 38 30.8 | −35 59 33 | 0.032 | 131.84 | 0.64 | Sb | S1 | 4300 |
| IC 1816 | 02 31 51.0 | −36 40 19 | 0.017 | 71.31 | 0.35 | SBa/b | S1 | ... |
| Mrk 0279 | 13 53 03.4 | +69 18 30 | 0.031 | 123.89 | 0.60 | Sa | S1.0 | 6860 |
| Mrk 0290 | 15 35 52.3 | +57 54 09 | 0.029 | 123.89 | 0.60 | E | S1.5 | 2550 |
| Mrk 0352 | 00 59 53.3 | +31 49 37 | 0.015 | 63.08 | 0.31 | E | S1.0 | 3800 |
| Mrk 0423 | 11 26 48.5 | +35 15 03 | 0.032 | 131.84 | 0.64 | Sb | S1.8 | 9000 |
| Mrk 0530 | 23 18 56.6 | +00 14 38 | 0.029 | 119.91 | 0.58 | Sa | S1.5 | 6560 |
| Mrk 0595 | 02 41 34.9 | +07 11 14 | 0.028 | 111.91 | 0.54 | Sa | S1.5 | 2360 |
| Mrk 0609 | 03 25 25.3 | −06 08 38 | 0.032 | 139.74 | 0.68 | Sa/b | S1.8 | ... |
| Mrk 0704 | 09 18 26.0 | +16 18 19 | 0.029 | 119.91 | 0.58 | SBa | S1.2 | 5500 |
| Mrk 0871 | 16 08 36.4 | +12 19 51 | 0.034 | 139.74 | 0.68 | Sb | S1.5 | 3690 |
| Mrk 0885 | 16 29 48.2 | +67 22 42 | 0.026 | 103.87 | 0.50 | SBb | S1.0 | ... |
| Mrk 1126 | 23 00 47.8 | −12 55 07 | 0.010 | 46.48 | 0.23 | Sb | S1.5 | ... |
| Mrk 1400 | 02 20 13.7 | +08 12 20 | 0.029 | 119.91 | 0.58 | Sa | S1.0 | ... |
| NGC 5252 | 13 38 15.9 | +04 32 33 | 0.022 | 95.79 | 0.46 | S0 | S1.9 | 2500 |
| NGC 5940 | 15 31 18.1 | +07 27 28 | 0.033 | 139.74 | 0.68 | SBc | S1.0 | 5240 |
| NGC 6212 | 16 43 23.1 | +39 48 23 | 0.030 | 123.89 | 0.60 | Sb | S1 | 6050 |
| IISZ 10 | 13 13 05.8 | −11 07 42 | 0.034 | 139.74 | 0.68 | ? | S1.5 | 3760 |

[a]From the bulge–disc decomposition, MRK 335 seems better described by a unique high Sérsic profile. This object is therefore rejected from our bulge analysis.
[b]From the bulge–disc decomposition, ESO 438G9 seems a bulgeless galaxy. This object is therefore rejected from our bulge analysis.

types. Putting this result into perspective with our bulge–disc decomposition suggests that the bulges of NLS1 hosts are likely to be 'pure' pseudo-bulges, while the bulges of BLS1 hosts appear to be composite bulges and hence have Sérsic indices distributed around $n_\mathrm{b} \sim 2.5$.

In order to test the significance of the difference between the Sérsic index distributions of NLS1s and BLS1s, we use the Kolmogorov–Smirnov test. As such, the cumulative distributions of the Sérsic index are presented in Fig. 3. The slopes of these distributions reflect the difference in the dispersions given above ($\sigma_n \sim$ 0.39 and 0.97 for the NLS1 and BLS1 samples, respectively). They emphasize that the population of NLS1 bulges appears to be like the population of pseudo-bulges, while the properties of the BLS1 bulges are more widely distributed between pseudo- and classical bulges. While we cannot fully reject the null hypothesis of the Kolmogorov–Smirnov test, it yields a probability of <1.2 per cent that the NLS1s and the BLS1s are drawn from the same parent distribution. This is a remarkable result that again underlines the connection between BH and bulge properties.

Since a result from Weinzirl et al. (2009) suggests a possible link between bars and bulges, we verify that the relative bar fractions in our samples have a minimum impact on our result of Fig. 2. Indeed, as described previously in Section 3.2, our selection of NLS1s and BLS1s respects the relative bar fraction observed, i.e. ∼25 per cent in BLS1 and ∼75 per cent in NLS1 galaxies. Therefore, we consider in Fig. 4 (right) the distribution of bulge Sérsic indices of NLS1 and BLS1 galaxies with bars only. While we observe a general small shift towards lower Sérsic indices (as expected from; e.g. Weinzirl

**Table 2.** Results of the bulge–disc decomposition for the NLS1s and BLS1s. Columns – (1): object name; (2): fitted components; the different components p, g, s, d, b stand, respectively, for PSF, Gaussian, Sérsic, disc (exponential) and background (sky); components are put in brackets if one or more of their parameters are kept fixed in the fit; (3): the $FWHM_g$ of the Gaussian component in kpc; (4): the bulge Sérsic index; (5): $R_b$, the effective radius of the bulge in kpc; (6): $R_d$, the scale radius of the disc in kpc; (7)–(8): axial ratio of the bulge and the disc components; (9)–(10): *B/D* and *B/T*, the bulge-to-disc and bulge-to-total luminosity ratios; (11): $\chi^2_\nu$, the reduced $\chi^2$ of the obtained fit. See also Appendix A.

| Object name | Comp. | $FWHM_g$ (kpc) | $n_b$ | $R_b$ (kpc) | $R_d$ (kpc) | $q_b$ | $q_d$ | *B/D* | *B/T* | $\chi^2_\nu$ |
|---|---|---|---|---|---|---|---|---|---|---|
| (1) | (2) | (3) | (4) | (5) | (6) | (7) | (8) | (9) | (10) | (11) |
| NLS1 sample | | | | | | | | | | |
| KUG 1136 | g+s+d+b | 0.07 | 1.21 | 0.95 | 3.15 | 0.76 | 0.62 | 0.20 | 0.17 | 1.16 |
| MRK 0042 | g+s+d+b | 0.07 | 1.27 | 0.44 | 3.12 | 0.82 | 0.58 | 0.21 | 0.18 | 0.95 |
| MRK 0335[a] | g+s+b | 0.18 | 3.41 | 1.27 | – | 0.93 | – | – | – | 1.20 |
| MRK 0359 | g+s+d+b | 0.08 | 1.41 | 1.19 | 7.45 | 0.67 | 0.83 | 0.12 | 0.11 | 1.03 |
| MRK 0382 | g+s+d+b | 0.12 | 1.36 | 0.52 | 3.02 | 0.94 | 0.54 | 0.46 | 0.31 | 1.49 |
| MRK 0493 | g+s+d+b | 0.08 | 0.74 | 0.34 | 3.74 | 0.97 | 0.41 | 0.17 | 0.15 | 1.02 |
| MRK 0766 | g+s+d+b | 0.06 | 1.88 | 0.15 | 1.21 | 0.74 | 0.44 | 0.13 | 0.11 | 1.05 |
| MRK 0896 | g+s+d+b | 0.10 | 2.06 | 0.37 | 2.82 | 0.77 | 0.71 | 0.18 | 0.15 | 1.34 |
| MRK 1044 | g+s+d+b | 0.07 | 1.45 | 0.20 | 1.18 | 0.91 | 0.76 | 0.44 | 0.30 | 1.05 |
| NGC 4748 | g+s+d+b | 0.07 | 1.93 | 0.25 | 1.89 | 0.98 | 0.68 | 0.25 | 0.20 | 0.68 |
| BLS1 sample | | | | | | | | | | |
| ESO 438G9[b] | g+d+b | 0.06 | – | – | 1.76 | – | 0.52 | – | – | 1.39 |
| F1146 | g+s+d+b | 0.07 | 3.74 | 0.90 | 2.09 | 0.47 | 0.65 | 1.22 | 0.55 | 1.54 |
| IC 1816 | g+s+[d]+b | 0.07 | 1.98 | 0.41 | [4.47] | 0.92 | 0.67 | 0.11 | 0.10 | 0.84 |
| Mrk 0279 | p+s+d+[b] | – | 2.18 | 2.48 | 11.11 | 0.58 | 0.56 | 0.57 | 0.36 | 0.97 |
| Mrk 0290 | g+s+d+b | 0.10 | 4.06 | 0.47 | 2.22 | 0.86 | 0.88 | 0.90 | 0.47 | 1.11 |
| Mrk 0352 | g+s+d+b | 0.05 | 4.49 | 0.90 | 1.59 | 0.98 | 0.76 | 0.79 | 0.44 | 0.84 |
| Mrk 0423 | [s+d]+b | – | 2.13 | 0.43 | 1.72 | 0.69 | 0.68 | 0.73 | 0.42 | 1.62 |
| Mrk 0530 | [g]+s+d+b | 0.17 | 2.4 | 1.04 | 4.04 | 0.85 | 0.65 | 0.60 | 0.38 | 0.75 |
| Mrk 0595 | g+s+[d]+b | 0.06 | 3.47 | 0.74 | 1.86 | 0.66 | [0.75] | 1.92 | 0.66 | 1.30 |
| Mrk 0609 | g+s+[d]+[b] | 0.15 | 2.28 | 1.48 | [2.53] | 0.79 | [0.95] | 1.60 | 0.62 | 2.52 |
| Mrk 0704 | g+s+d+b | 0.16 | 2.88 | 1.19 | 6.29 | 0.70 | 0.50 | 0.75 | 0.43 | 1.25 |
| Mrk 0871 | g+s+d+b | 0.12 | 1.28 | 0.61 | 3.78 | 0.52 | 0.38 | 0.13 | 0.11 | 0.91 |
| Mrk 0885 | g+s+d+b | 0.07 | 2.62 | 2.70 | 9.05 | 0.74 | 0.52 | 0.32 | 0.24 | 0.83 |
| Mrk 1126 | g+s+d+b | 0.04 | 1.86 | 0.27 | 1.78 | 0.86 | 0.66 | 0.17 | 0.15 | 0.47 |
| Mrk 1400 | g+s+d+b | 0.12 | 1.7 | 0.55 | 2.27 | 0.61 | 0.31 | 0.32 | 0.24 | 0.98 |
| NGC 5252 | g+s+d+b | 0.07 | 3.9 | 2.42 | 3.20 | 0.53 | 0.44 | 0.58 | 0.37 | 0.35 |
| NGC 5940 | g+s+d+b | 0.10 | 1.23 | 0.30 | 3.77 | 0.89 | 0.66 | 0.06 | 0.06 | 0.99 |
| NGC 6212 | g+s+d+b | 0.09 | 1.52 | 1.23 | 2.88 | 0.75 | 0.70 | 0.77 | 0.43 | 0.87 |
| IISZ 10 | g+s+d+b | 0.18 | 1.92 | 1.56 | 4.29 | 0.91 | 0.72 | 0.70 | 0.41 | 0.57 |

[a]From the bulge–disc decomposition, MRK 335 seems better described by a unique high Sérsic profile. This object is therefore rejected from our bulge analysis.
[b]From the bulge–disc decomposition, ESO 438G9 seems a bulgeless galaxy. This object is therefore rejected from our bulge analysis.

et al. 2009), NLS1 and BLS1 are clearly distinct. Following this observation, we reasonably conclude that although the presence of a bar can be linked to the bulge Sérsic index, it does not imply that the bulge is a pseudo-bulge. Thus, our result that NLS1s tend to possess pure pseudo-bulges in contrast to BLS1s is not a consequence of different bar fractions in the two populations.

Finally, we consider the influence of the Seyfert type of the BLS1s on our Sérsic measurements. Indeed, changes from type 1 to intermediate-type Seyferts can be attributed to changes in the ionizing radiation of the AGN (e.g. Goodrich 1990), or to variation in the absorbing material (Maiolino & Rieke 1995; Forster 1999), or as well to different inclination of the host galaxies (e.g. Maiolino & Rieke 1995; Ramos Almeida et al. 2009). These effects can explain the large Balmer decrements in the optical spectra of intermediate-type galaxies but can also indirectly bias our Sérsic index measurements. Indeed, in the case of intermediate-type Seyferts, a fainter AGN would ease the fit, but an excess of dust in the host galaxy and projection effects (nearly edge-on host spirals) can make fitting the host harder. For these reasons, we check whether there is any systematic effect on our fits by looking at the Sérsic index versus the Seyfert type of the BLS1s (given in Table 1), the result is given Fig. 4 (left). Since no trend of the Sérsic index with the BLS1 subclass can be observed, we can be confident that our fits are not biased by systematic effects related to the intermediate BLS1 classifications.

Similarly, NLS1s are a subclass of type 1 AGN, for which the Seyfert subclassification is based solely on the properties of the AGN itself. But our result also shows that the bulge properties of the NLS1 host galaxies do represent a distinct subclass of the bulges of BLS1 hosts.

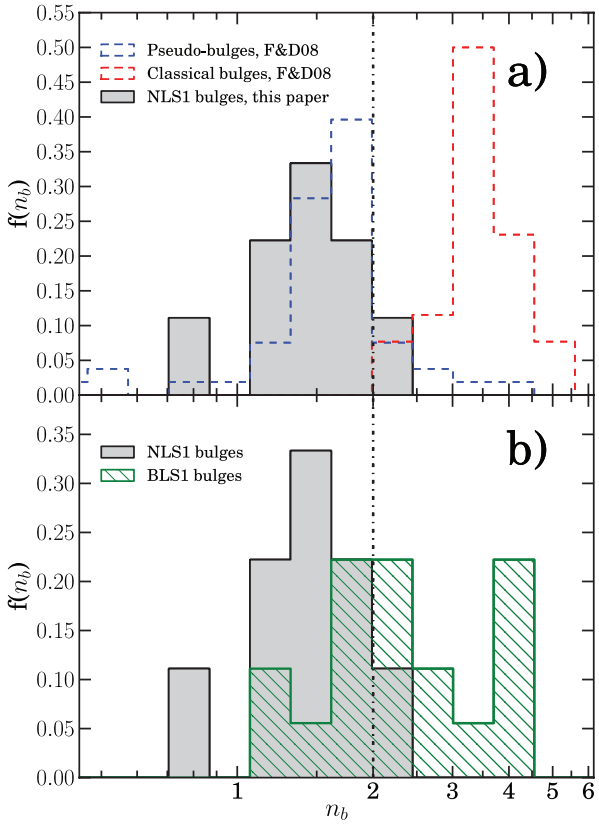


**Figure 2.** Histogram of bulge Sérsic indices, $n_b$. (a) NLS1 host bulges (nine objects) from our sample compared to pseudo-bulges (53 objects) and classical bulges (26 objects, we do not include their sample of elliptical galaxies) from Fisher & Drory (2008). (b) NLS1 host bulges compared to BLS1s host bulges (18 objects).

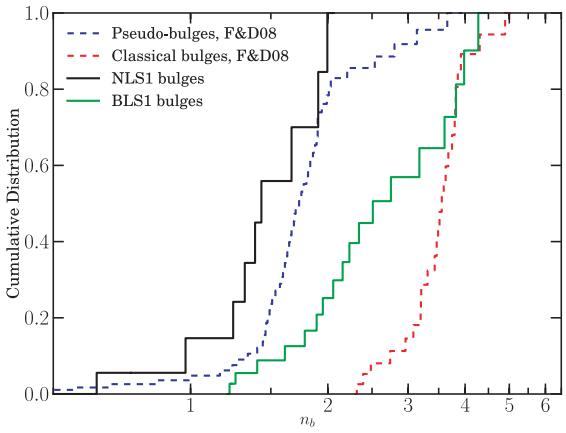


**Figure 3.** Cumulative distribution versus the Sérsic index for pseudo- and classical bulges (Fisher & Drory 2008), and NLS1 and BLS1 host bulges (this paper).

### *3.3.2 Bulge prominence and Fundamental Plane projections*

Building on our fit results, we study the bulge prominence by looking at the size distribution of the bulges, as well as the bulge-to-disc (*B*/*D*) and bulge-to-total (*B*/*T*) light ratios. The first objective here is to further explore the differences between NLS1 and BLS1 host bulges. But doing so also enables us to confirm the validity of our bulge–disc decomposition.

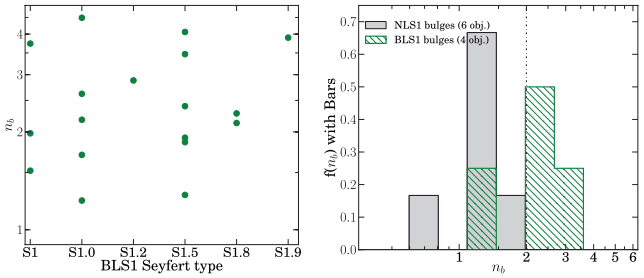


**Figure 4.** Left: BLS1 Seyfert type versus their respective Sérsic index. Since there is no trend, the Sérsic index does not seem affected by the Seyfert classification of our BLS1s. Right: histogram of bulge Sérsic indices, $n_b$, of NLS1 (six objects) and BLS1 (four objects) barred galaxies; see also Table 1 for the classification and Table 2 for $n_b$.

We compute the *B*/*D* and *B*/*T* light ratios using our fit parameters (see equations A3 and A4) given in Table 2, and present their distribution in Fig. 5 (left). The median *B*/*T* of 0.39 in BLS1s and 0.17 in NLS1s indicates that NLS1 galaxies have lower *B*/*T* light ratios than BLS1s. We compare these distributions to $\langle B/T \rangle = 0.41$ for an average classical bulge and $\langle B/T \rangle = 0.16$ for an average pseudo-bulge given by Fisher & Drory (2008). Gadotti (2009) also finds similar values. The *B*/*T* ratio therefore provides strong support for our conclusion that NLS1 bulges are pseudo-bulges, while BLS1 bulges are largely composite or classical.

In the same Fig. 5 (right), we also plot the *B*/*T* light ratios versus the Hubble type, the Sérsic index and the effective radius of the bulges. As expected, the mean *B*/*T* ratio tends to decrease with the Hubble type (e.g. Graham & Worley 2008; Masters et al. 2010), and hence it appears that NLS1 galaxies tend to be of later type than BLS1 galaxies (Fig. 5, left). The two last plots illustrate again that NLS1 bulges have less prominent (i.e. smaller, fainter, less cuspy) bulges than BLS1 bulges.

While the Sérsic index is a convincing tool to distinguish pseudo-bulges from classical bulges (Fisher & Drory 2008), Gadotti (2009) uses the Kormendy relation ($\langle \mu_e \rangle$–$r_e$) to identify pseudo-bulges as fainter bulges than predicted by the Fundamental Plane of elliptical galaxies. In Fig. 6, we present the Kormendy relation, the surface brightness magnitude at the effective radius and the Sérsic index versus the effective radius of the bulge. For Figs 6(a) and (b) we have overdrawn linear fits to the data for the BLS1 sample. While these do not reveal any marked offset between the two NLS1 and BLS1 classes, NLS1 bulges are systematically fainter than those of BLS1 (i.e. they tend to lie under the line). This result is consistent with the common structural properties we are finding for the NLS1 class. Finally, Fig. 6(c) shows NLS1 and BLS1 host bulges, together with pseudo- and classical bulges (from Fisher & Drory 2008) in the $n_b$–$r_e$ plane. Again, it shows clearly that NLS1s lie in the region occupied by pseudo-bulges, while BLS1 are spread over the whole range of pseudo- and classical bulge properties.

Finally, we also look at the distribution of Sérsic indices with the FWHM of the broad component of H$\beta$ in Fig. 7. While the sample is not large enough to make conclusive remarks, we note the existence of a correlation of the FWHM with the Sérsic index, confirmed by a Spearman's rank correlation coefficient of ∼0.49. This correlation indicates, at least in the low FWHM(H$\beta$) range, a possible connection between the bulge concentration and the BLR.

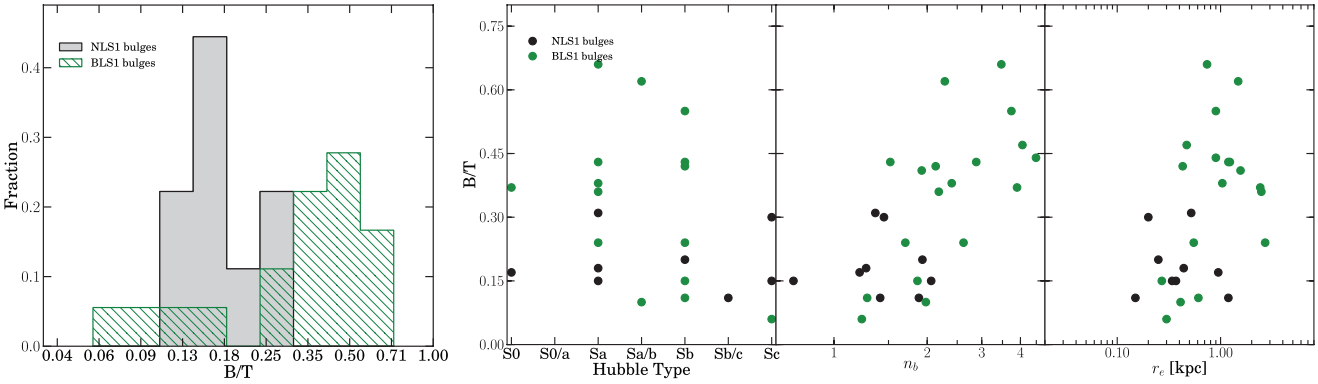


**Figure 5.** Left: distribution of bulge-to-total light ratio in NLS1 and BLS1s galaxies. According to e.g. Masters et al. (2010), NLS1 galaxies would therefore be later type galaxies than BLS1. Right: verification of the mean *B*/*T* decrease with the Hubble type, *B*/*T* against the bulge Sérsic index and against the bulge effective radius. The two last plots confirm the link between *B*/*T* light ratios and the prominence of the bulge.

### *3.3.3 Complementary studies*

Three other studies support our conclusion about the bulges of NLS1s.

In studying the central engines of NLS1 galaxies, Ryan et al. (2007) perform a bulge–disc decomposition of 11 NLS1s galaxies with $z \leq 0.05$ in the $J$ and $K_s$ band using adaptive optics data from the 3.6-m Canada–France–Hawaii Telescope (CFHT). Their mean Sérsic indices are $\langle n_J \rangle = 1.52$ and $\langle n_K \rangle = 1.38$, and standard deviations $\sigma_n$ of ∼0.44 and ∼0.48, respectively. As the Sérsic index seems to be, at most, weakly correlated to the photometric band (see e.g. Fisher & Drory 2008, who compare the Sérsic index in the $V$ and $H$ bands), the Ryan et al. decomposition supports our results.

In studying low BH mass systems, Greene, Ho & Barth (2008) argue that most of their disc galaxies have pseudo-bulges. Since these systems have small FWHM(H$\beta$), they are also likely to be NLS1s although the relative Fe II strengths they found are lower than in classical NLS1s (Greene & Ho 2004).

In a more recent paper, Mathur et al. (2011) study 10 NLS1 galaxies [Advanced Camera for Surveys/High-Resolution Channel (ACS/HRC) using the *F625W* filter]. They perform a similar bulge–disc decomposition (i.e. they fit a Sérsic profile for the bulge and an exponential profile for the disc), and also conclude that they have pseudo-bulges. While our conclusions are based mainly on the Sérsic index, they use the Kormendy relation, as advised by Gadotti (2009), to conclude on the pseudo-bulge nature of NLS1 bulges. Indeed, they do not find systematically low Sérsic indices but obtain a mean Sérsic index of $\langle n \rangle = 2.61$ and a large Sérsic index dispersion $\sigma_n = 1.82$. In fact only six out of the 10 galaxies in their sample have Sérsic index values consistent with pseudo-bulge profiles. To try and understand this difference, we note that the Mathur et al. (2011) sample differs from that presented by us here. Specifically, their sample is found at larger redshift, $\langle z \rangle \sim 0.24$, leading to a scale in kpc arcsec$^{-1}$ on average ∼four times larger than in our sample. A large scale limits how well the fit is constrained by the central regions, and confusion in the light distributions between the nucleus and the bulge may arise, possibly leading to higher Sérsic indices.

One caveat to these works is the lack of a comparison sample of BLS1 hosts, which our results show is important. By including one, we show that one should consider the hosts of NLS1s to be a subset of all BLS1s, rather than being totally separate. The distinction between NLS1 and BLS1 hosts is thus that while NLS1 hosts specifically have pseudo-bulges, BLS1 hosts have a range of bulge types including pseudo-bulges, composite bulges and classical bulges.

### 3.4 Secular evolution has always prevailed

The Sérsic index distribution and the prominence of the bulge both indicate that, statistically, NLS1 hosts have 'pure' pseudo-bulges, in contrast to BLS1 galaxies. The consequence of this result (Kormendy & Kennicutt 2004) is that internal secular processes must have dominated the past evolution of NLS1 hosts. And, therefore, it is from this perspective that one should attempt to explain the particular AGN properties observed in NLS1 galaxies (such as low BH mass, high accretion rates, etc.).

## 4 NLS1 EVOLUTION AND BLACK HOLE GROWTH

We explore here the implications of our conclusion that secular processes have dominated the evolution of NLS1 galaxies. We focus on the issue of the BH growth of NLS1s, and in understanding whether or not NLS1 galaxies are in a special phase of BH growth.

### 4.1 Expected galaxy populations that have evolved through secular evolution

Over the last few years, the relative importance of major mergers versus minor mergers and secular processes in driving galaxy formation and evolution has become a key issue in simulations and semi-analytic models. Genel et al. (2008) and Parry, Eke & Frenk (2009) offer two different perspectives to understanding the growth processes of dark matter haloes and galaxies. Both studies conclude that major mergers are not necessarily the main driver of galaxy mass evolution.

Genel et al. (2008) investigate, by analysing cosmological simulations, the growth of dark matter haloes. They extract halo merger fractions and mass accretion rates from the Millennium Simulation in order to study the possible role of major mergers in the evolution of haloes from $z \sim 2$ to 0. Following the fate of haloes in the mass range $11.5 \leq \log M_{z=2.2} \leq 12.8$, they find that ∼1/3 of haloes which reach $z = 0$ have not undergone any major mergers since $z \sim 2.2$ and that such haloes gain $\gtrsim 70$ per cent of their new mass via mergers less intense than 1:10, demonstrating the importance of non-major merger processes. In a following paper, Genel et al. (2010) also

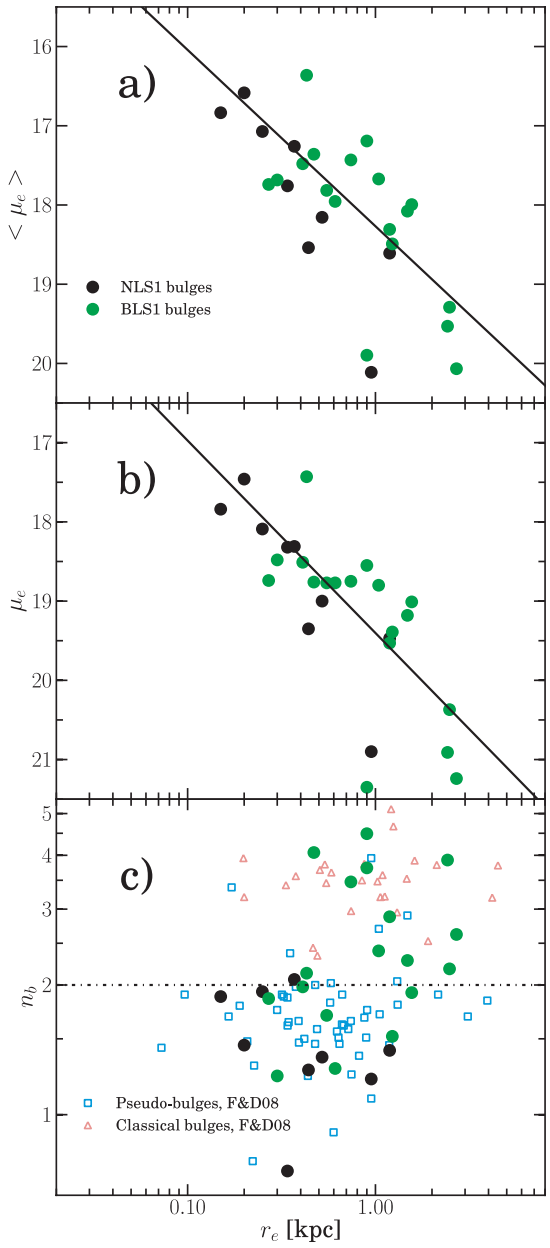


**Figure 6.** Relations of bulge parameters with the effective radius $r_e$ of the bulges. (a) Kormendy relation, i.e. the mean surface brightness magnitude within the effective radius versus $r_e$. (b) Surface brightness magnitude at the effective radius versus $r_e$. The solid lines are the linear fit found for BLS1s from our sample. The magnitudes are given in the STMAG system. (c) Effective radius versus Sérsic index comparing classical- and pseudo-bulges from Fisher & Drory (2008) with our samples of NLS1s and our BLS1s. The NLS1s seem to lie at the expected $r_e$–$n_b$ of typical pseudo-bulges.

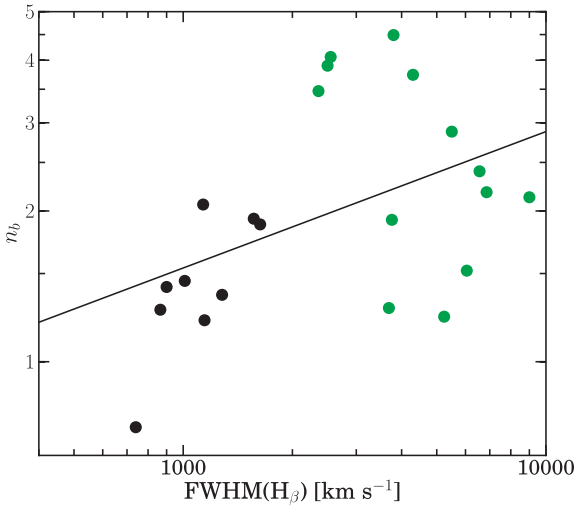


**Figure 7.** FWHM versus Sérsic index. NLS1s and BLS1s are represented by black and green dots, respectively. The linear fit is based on the two samples. The Spearman's rank correlation coefficient is ∼0.49.

show that, independently of halo mass, ∼40 per cent of the mass in haloes have been assembled through smooth accretion.

Parry et al. (2009) study galaxy growth by analysing two different galaxy formation models, both also based on the Millennium Simulation. Their statistical results are revealing. For both models, they find that only ≤49 per cent of ellipticals, ≤3 per cent of S0s and ≤2 per cent of spirals undergo a main branch major merger (mass ratio greater than 1:3) in their entire formation history. In other words, ∼98 per cent of spiral galaxies – which are the most common morphological type of NLS1s host galaxies – do not undergo any major merger. These results are largely independent of total stellar mass of the galaxy except for ellipticals. In a further step, they quantify the relative impact of disc instabilities, major mergers and minor mergers on galaxy morphology by determining the stellar mass fraction from each process as a function of the total stellar mass. For both models, they find that instabilities and minor mergers are the main mass contributor, with their relative contributions depending on the treatment of disc instabilities in the models (see Parry et al. 2009 and references therein).

While it is beyond the scope of this paper to discuss the treatment of the various physical processes in these galaxy formation models, one clear conclusion is that even hierarchical cosmological simulations give rise to large galaxy populations that have evolved through secular processes. Interestingly, observational studies also reach similar conclusions.

Weinzirl et al. (2009) study present-day ($D < 60$ Mpc) spiral galaxies. By performing two-dimensional multicomponent decompositions of 143 high-mass ($M \geq 10^{10}\,M_\odot$) spirals, they analyse the bulge Sérsic index and $B/T$ distributions. Their results highlight the large fraction of bright spirals having $B/T \leq 0.2$ (∼69 per cent) and $n \leq 2$ (∼76 per cent) where many of them host bars (∼66 per cent). By comparing their result to theoretical predictions, they find that ∼66 per cent of present-day high-mass spirals have not undergone a major merger since $z \leq 2$ and likely not even since $z \leq 4$. This conclusion conveys the importance of minor mergers (in the present case for a mass ratio <1:4) and secular processes since $z \leq 4$.

Finally, Cisternas et al. (2011) recently analysed the relevance of different triggering mechanisms for AGN activity. Based on visual analysis of 140 AGN and 1264 inactive galaxies with *HST* imaging, they measure the fraction of distorted morphologies which they take to be a signature of recent mergers. They conclude that the bulk of BH accretion has been triggered by secular processes and minor interactions since $z \sim 1$.

By assessing the role of secular processes, these various theoretical and observational lines of evidence offer a cosmological context to our conclusions concerning NLS1 hosts. They show that a significant fraction of galaxy mass and a large number of galaxies have evolved from early cosmic times without any mergers. It is reasonable to suggest that NLS1s, which our analysis shows must

have evolved without mergers, may be tracers of this population of galaxies. Our attempt, in the rest of this section, to put this hypothesis on a more quantitative basis leads us to an estimate of the duty cycle of NLS1s.

### 4.2 How common are NLS1s?

In the last decade, various surveys of nearby galactic nuclei have found that the fraction of objects classified as AGN is surprisingly large. They show that, of all local galaxies, approximately 10 per cent are Seyferts and 40 per cent can be considered active (see Ho 2008 and references therein).

Looking at the NLS1s, several surveys using optical and X-ray selected samples (e.g. Williams et al. 2002; Crenshaw et al. 2003; Zhou et al. 2006) find that they make up approximately 15 per cent of Seyfert 1 galaxies. Based on the unified AGN scenario, one can expect that this fraction should apply also to type 2 Seyferts: that ∼15 per cent of Seyfert 2 galaxies may have narrow broad emission lines that are hidden from sight by the obscuring torus. Such a possibility has already been suggested by Zhang & Wang (2006), who argue that Seyfert 2s without a hidden BLR (i.e. one that cannot be observed in polarized light) are the counterparts of NLS1s. Taking this further, one could reasonably argue that the NLS1 definition might extend even to the lower luminosity AGN.

Combining these fractions together leads to the assessment that 2–6 per cent of local galaxies could be 'NLS1-like' galaxies, i.e. active galaxies with 'narrow' broad lines whether obscured or not, the evolution of which has been dominated at all cosmic times by secular processes.

### 4.3 Duty cycle of NLS1 black holes

Our analysis in Section 3 shows that NLS1 galaxies statistically have a bulge Sérsic index $n_{\rm b} < 2$ and a bulge-to-total light ratio $B/T < 2$. The observational study of Weinzirl et al. (2009), corroborated by the theoretical study of Parry et al. (2009), argues that approximately 2/3 of local spiral galaxies[3] have similar properties to NLS1 hosts. Assuming that each galaxy among this population can potentially undergo nuclear activity and become 'NLS1-like',[4] we can estimate the duty cycle of NLS1s. We argue above that 'NLS1-like' objects may comprise as much as ∼6 per cent of local galaxies (note that we use the upper end of the range above in order to be conservative later in our estimates of BH growth). This implies that their duty cycle should be around ∼9 per cent.

Since the Hubble sequence formed at $z \sim 1$ (van den Bergh et al. 2000; Kajisawa & Yamada 2001; Conselice et al. 2004; Cassata et al. 2010; Oesch et al. 2010) with bars becoming numerous at this redshift (Abraham et al. 1999; Sheth et al. 2003, 2008; Elmegreen, Elmegreen & Hirst 2004; Jogee et al. 2004; Marinova & Jogee 2007), accretion driven by large-scale bars can only have occurred in the last ∼7.7 Gyr. With a duty cycle of ∼9 per cent, this means that NLS1s have actively accreted on to their BHs for ∼690 Myr.

Assuming their BHs are accreting at the Eddington rate, the e-folding time of their BH build-up is given by the Eddington timescale, $t_{\rm E} \approx 4.4 \times 10^8$ yr. Therefore, the BH mass increase is given by (e.g. Volonteri 2010)

$$M_{\rm BH}(t) = M_{\rm BH}^{\rm seed}(t_0) \exp\left(\frac{1-\epsilon}{\epsilon}\frac{\tau}{t_{\rm E}}\right), \quad (1)$$

where $t$ is the current (observed) time, and $\tau = t - t_0$ is the total accretion duration since the initial time $t_0$. The radiative efficiency $\epsilon$ is a key parameter, and can have a major impact on the BH growth rate because it is inside the exponential term. The standard value of $\epsilon$ is ∼0.1. Adopting this then, and assuming a seed mass $M_{\rm BH}^{\rm seed}(t_0) = 10^3$–$10^4\,{\rm M}_\odot$, the current mass $M_{\rm BH}(t)$ could range from $10^9$ to $10^{10}\,{\rm M}_\odot$. On the other hand, accretion on to a fast rotating Kerr BH can lead to a radiative efficiency $\epsilon \sim 0.2$ or higher (Volonteri et al. 2005; Jogee 2006). For the same $M_{\rm BH}^{\rm seed}(t_0)$, this higher radiative efficiency implies a much slower BH growth and leads to current BH masses between $5 \times 10^5$ and $5 \times 10^6\,{\rm M}_\odot$.

Based on these very simple estimates, we reach two conclusions. First, NLS1s are not necessarily in a special phase of their BH growth. Their BHs have required 7–8 Gyr to grow to their current size. To increase their BH mass by another factor of 10 requires – for a 9 per cent duty cycle and $\epsilon = 0.2$ – another ∼2.8 Gyr. Thus, despite their high Eddington ratios, NLS1s are not imminently evolving into BLS1s, although they may do this eventually. Secondly, the low BH masses of NLS1s (with respect to BLS1s) can easily be accounted for by a high radiative efficiency. The theoretical and observational evidence for rapidly spinning BHs in NLS1s is the topic of the Section 5.1.

## 5 DISCUSSION

### 5.1 NLS1s and highly spinning black holes

As discussed in the last paragraph, the radiative efficiency of the AGN have a direct impact on their BH growth and their final BH masses. But radiative efficiency is determined by the supermassive black hole (SMBH) spin, which in turn is influenced by the AGN accretion history. Different scenarios have been studied where SMBH spins evolve through mergers, subsequent prolonged accretion (constant angular momentum axis of the accreting material; e.g. Volonteri et al. 2005; Berti & Volonteri 2008) or chaotic accretion (random disc orientations with respect to the BH; e.g. King & Pringle 2007; Berti & Volonteri 2008; King, Pringle & Hofmann 2008). Volonteri et al. (2005) and Berti & Volonteri (2008) have shown that if major and minor BH mergers are the sole source of material, then the distribution of BH spins in a $z = 0$ galaxy population will reflect that of the initial seed BH spin. In contrast, they find that prolonged gas accretion triggered by galaxy mergers tends to spin BHs up, and that galaxies where a significant fraction of the BH growth occurs in this mode could have maximal BH spin. However, in such a case, most distant quasars would have high radiative efficiency and would inefficiently grow their BH. This would require massive BH seeds, in conflict with the Soltan argument. If instead, the accretion proceeds by short randomly oriented events (King & Pringle 2007; King et al. 2008), then the spins will tend to be low and lead to high BH masses, resolving the conflict with the Soltan argument. However, NLS1 BHs are likely fed via secular rather than merger processes, therefore, the angular momentum of the infalling matter could be related to the host structure and hence have a favoured direction. NLS1 SMBHs could be evolving through the prolonged gas accretion scenario. Therefore, NLS1 secular evolution would imply high spins and low BH masses.

[3] High mass ($M_\star \geq 1.0 \times 10^{10}\,{\rm M}_\odot$) low-to-moderately inclined ($i < 70^\circ$) spirals.

[4] Clearly the 2/3 of the local galaxies are not necessarily potential true NLS1s; but, given that their hosts appear to have evolved over cosmic time in a similar way, they might be 'NLS1 like', as defined in Section 4.2, during their accretion phase.

From an observational point of view, it appears to be possible to derive BH spins using the Fe K$\alpha$ line in the hard X-ray continuum using accretion disc reflection models. While there are several potential reasons that might prevent one from obtaining a good spin constraint for a given source (such as too few photons, or too narrow iron line hampering the fit to pick out the role of relativistic contributors; Brenneman 2007) several recent works have been able to derive formal constraints on BH spin for a number of Seyfert galaxies (e.g. Brenneman 2007; Fabian et al. 2009; Miniutti et al. 2009; Ponti et al. 2010). Among these measurements, we find that most of them are for NLS1s, and that the derived spin values are very high. While there are still too few measurements to draw any firm conclusion, these results are already suggestive that NLS1s could have highly spinning BHs owing to the prolonged disc accretion on to their BHs.

Finally, as we have already touched on in Section 4.3, a high spin leads to a high mass-to-energy conversion or radiative efficiency (because the last stable orbit is closer to the horizon of the BH), and hence to a slow BH growth. Therefore, the high Eddington ratio typically observed in NLS1s could be a signature not just of highly accreting BHs, but also of rapidly spinning BHs. Given that pseudo-bulges are one consequence of secular evolution in a galaxy, and that another consequence is that the SMBH should be rapidly spinning, our result that NLS1 hosts have pseudo-bulges leads to the prediction that a large fraction of NLS1 BHs should have very high spin. Future X-ray missions may be able to test this.

### 5.2 Black hole–bulge scaling relation

One question concerning NLS1s that has received much attention is whether they follow the $M_{\rm BH}$–$\sigma_\star$ relation or are offset under it. The $M_{\rm BH}$–$\sigma_\star$, or more generally the BH–bulge scaling relations, are often interpreted as physical evidence for the co-evolution of the central BHs with the galactic bulges. The case of NLS1s is rather controversial. On one hand, many studies suggest they may reside below the relation, in which case they could be evolving on to it (e.g. Mathur, Kuraszkiewicz & Czerny 2001; Bian & Zhao 2004; Grupe & Mathur 2004; Mathur & Grupe 2005a,b; Zhou et al. 2006). On the other hand, several different studies place them on the relation once contaminating effects have been corrected for, such as [O III] line[5] broadening due to outflows (see Botte et al. 2005; Komossa & Xu 2007), or radiation pressure (as proposed by Marconi et al. 2008).

Current developments regarding the $M_{\rm BH}$–$\sigma_\star$ relation highlight that it may not be universal (common to all morphological types), and that perhaps one should distinguish between barred and barless galaxies, discs and ellipticals (e.g. Graham 2008; Hu 2008; Graham & Li 2009; Graham et al. 2011), classical bulges and pseudo-bulges (e.g. Nowak et al. 2010; Kormendy, Bender & Cornell 2011; Sani et al. 2011). In fact, barred, disc galaxy bulges and pseudo-bulges appear either to lie below the relation or to scatter around it. Additionally, on a more theoretical side, some authors (Peng 2007; Jahnke & Macciò 2011) suggest that the BH–bulge scaling relations could be non-causal (their origin would not invoke a physical coupling between the SMBH and the galaxy) but rather would be naturally produced by the merger-driven assembly of bulge and BH masses, and therefore galaxies with pseudo-bulges would not be expected to obey the same relation (Jahnke & Macciò 2011).

[5] This line is often used as a surrogate of the stellar dispersion $\sigma_\star$, see Nelson (2000).

Our result that NLS1s have pseudo-bulges suggests that we should expect these AGN to lie in the same region as inactive galaxies with pseudo-bulges, that is scattered around and below the $M_{\rm BH}$–$\sigma_\star$ relation. It is not yet understood how – or whether – BH and bulge growth are linked when secular processes drive their evolution. Thus, while it is clear that their BHs are still growing, we cannot predict where they will end up on the $M_{\rm BH}$–$\sigma_\star$ plane.

### 5.3 Evolutionary scenarios

Several authors have suggested different links between NLS1 galaxies and other AGN types in evolutionary sequence contexts. We briefly discuss them in the light of our results.

Mathur (2000) argues that NLS1 galaxies might be in an early stage of evolution owing to their small growing BHs and higher Eddington rates. This proposition is not inconsistent with our results. Nevertheless, it illustrates a different perspective. Either NLS1s would have their nuclear SMBHs recently formed and NLS1s would be young objects evolving into BLS1s (Mathur 2000; Mathur et al. 2011), or NLS1s would not be in any special phase of their evolution but simply have BHs that are growing slowly due to their duty cycle and spin. However, both perspectives agree that NLS1s galaxies have pseudo-bulges and that their BH growth is driven by secular processes as opposed to mergers at high redshift.

Kawakatu, Imanishi & Nagao (2007) proposed an evolutionary track from type 1 ultraluminous infrared galaxy (ULIRG), to NLS1 to BLS1. The connection between ULIRG and NLS1 appears contradictory with our results. Indeed, local ULIRGs are the result of galaxy mergers, while we have argued that, based on the host properties, NLS1s have a secular-driven evolution.

Zhang & Wang (2006) study Seyfert 2s with and without a hidden BLR (i.e. presence or absence of BLR in polarized light) and suggest that non-HBLR Seyfert 2s are the counterparts of NLS1s viewed at high inclination angles. In their subsequent paper, Wang & Zhang (2007) propose an evolutionary sequence of the narrow objects to broad-line AGN considering time evolution of the BH mass and the accretion rates. While it is not inconsistent with our results, the distribution of bulge properties in BLS1s suggests that not all BLS1s come from NLS1s that have evolved secularly, but that the BLS1 population should include galaxies that have undergone interactions and mergers. While Wang & Zhang (2007) propose a secular evolution from NLS1s to BLS1s (NLS1s would be an early AGN phase and would evolve to BLS1s during the AGN activity time), Zhu, Zhang & Tang (2009) proposed a similar scenario, but where NLS1s would be produced by mergers of smaller galaxies compared to BLS1s and could evolve to BLS1s only if they encounter more mergers to grow them. This last scenario appears contradictory to the results of the present paper.

While at this point there is no consensus on the cosmic evolution of NLS1s, our results suggest that they are a special case in which the evolution has been dominated at all time by secular processes. Thus, if the BHs in NLS1s continue to grow, they must eventually become broad-line AGN, and thus become part of the BLS1 population. However, our results also show very clearly that not all BLS1s have grown in this way, and that mergers have played a role in the evolution of the BLS1 population. In this respect, perhaps the most enlightening question would be: when NLS1s evolve into BLS1s, will they be distinguishable from systems classified as BLS1s but having undergone galaxy interactions and mergers? Perhaps one can already begin to address this by studying the BLS1s with pure pseudo-bulges, and asking whether they have definable characteristics that differ from the BLS1 population as a whole.

## 6 CONCLUSIONS

From a review of the literature, we show that secular evolution in NLS1 galaxies is a powerful and on-going process on all scales, in contrast to BLS1 galaxies. To assess the role of secular processes in the past evolution of NLS1 galaxies, we examine their bulge properties by performing bulge–disc decompositions on NLS1 and BLS1 galaxies with archival *HST* images. The results indicate that NLS1 host bulges are pseudo-bulges and distinct from the much broader population of BLS1 bulges. From these results, we conclude that NLS1s represent a class of AGN in which the BH growth is, and has always been, dominated by secular evolution.

Such an evolutionary mode signifies also a different BH growth mode in NLS1s than in merger-built systems. Interestingly, simulations of prolonged disc-mode gas accretion on to BHs show that the most efficient way to spin-up a BH is through smooth accretion of material. In this light, our results suggest that NLS1 galaxies should possess highly spinning BHs which is indeed what has so far been observed.

Our picture of the NLS1 galaxy phenomenon can be expressed as follows. The activity in NLS1 galaxies is, and always has been, powered by internal secular processes. This has lead to the growth of a pseudo-bulge. It is also characterized by a disc-mode accretion on to the central object, which tends to spin-up the BH. This leads to high radiative efficiency of the accreting material, therefore, reducing the actual mass accreted on to the BH and slowing its growth. The high radiative efficiency could in part explain the high Eddington ratios and small BH masses of NLS1s.

This picture can be tested by analysing the angular momentum in NLS1 bulges to assess definitively their pseudo-bulge nature. And studying the kinematics in the central part of NLS1s would help to understand how gas is transported to their central regions, what the mass inflow rates are and the role played by angular momentum. In parallel, systematic measurements of BH spins by future X-ray missions would also shed light on the growth of their BHs at the smallest scales.

## ACKNOWLEDGMENTS

We thank E. Sani and S. Mathur for useful discussions. We are grateful to an anonymous referee, A. Barth, E. Cameron, A. Graham, K. Jahnke, A. King and B. Simmons for useful and interesting comments. GOdX acknowledges support from and participation in the International Max-Planck Research School on Astrophysics at the Ludwig-Maximilians University. This research has made use of the NASA/IPAC Extragalactic Database (NED) which is operated by the Jet Propulsion Laboratory, California Institute of Technology, under contract with the National Aeronautics and Space Administration.

## REFERENCES

Abraham R. G., Merrifield M. R., Ellis R. S., Tanvir N. R., Brinchmann J., 1999, MNRAS, 308, 569
Acosta-Pulido J. A., Vila Vilaro B., Perez-Fournon I., Wilson A. S., Tsvetanov Z. I., 1996, ApJ, 464, 177
Berti E., Volonteri M., 2008, ApJ, 684, 822
Bian W., Zhao Y., 2004, MNRAS, 347, 607
Boller T., Brandt W. N., Fink H., 1996, A&A, 305, 53
Boroson T. A., 2002, ApJ, 565, 78
Botte V., Ciroi S., di Mille F., Rafanelli P., Romano A., 2005, MNRAS, 356, 789
Brenneman L. W., 2007, PhD thesis, Univ. Maryland, College Park
Caon N., Capaccioli M., D'Onofrio M., 1993, MNRAS, 265, 1013
Cassata P. et al., 2010, ApJ, 714, L79
Ciotti L., Bertin G., 1999, A&A, 352, 447
Cisternas M. et al., 2011, ApJ, 726, 57
Conselice C. J. et al., 2004, ApJ, 600, L139
Crenshaw D. M., Kraemer S. B., Gabel J. R., 2003, AJ, 126, 1690
Deo R. P., Crenshaw D. M., Kraemer S. B., 2006, AJ, 132, 321
Elmegreen B. G., Elmegreen D. M., Hirst A. C., 2004, ApJ, 612, 191
Fabian A. C. et al., 2009, Nat, 459, 540
Fisher D. B., Drory N., 2008, AJ, 136, 773
Fisher D. B., Drory N., 2010, ApJ, 716, 942
Forster K., 1999, PhD thesis, Columbia University
Gadotti D. A., 2009, MNRAS, 393, 1531
Genel S. et al., 2008, ApJ, 688, 789
Genel S., Bouché N., Naab T., Sternberg A., Genzel R., 2010, ApJ, 719, 229
Goodrich R. W., 1990, ApJ, 355, 88
Graham A. W., 2008, ApJ, 680, 143
Graham A. W., Li I.-H., 2009, ApJ, 698, 812
Graham A. W., Worley C. C., 2008, MNRAS, 388, 1708
Graham A. W., Onken C. A., Athanassoula E., Combes F., 2011, MNRAS, 412, 2211
Greene J. E., Ho L. C., 2004, ApJ, 610, 722
Greene J. E., Ho L. C., Barth A. J., 2008, ApJ, 688, 159
Grupe D., 2004, AJ, 127, 1799
Grupe D., Mathur S., 2004, ApJ, 606, L41
Ho L. C., 2008, ARA&A, 46, 475
Ho L. C., Filippenko A. V., Sargent W. L. W., 1997, ApJ, 487, 591
Hu J., 2008, MNRAS, 386, 2242
Jahnke K., Macciò A. V., 2011, ApJ, 734, 92
Jogee S., 2006, in Alloin D., ed., Lecture Notes in Physics Vol. 693, Physics of Active Galactic Nuclei at All Scales. Springer-Verlag, Berlin, p. 143
Jogee S. et al., 2004, ApJ, 615, L105
Kajisawa M., Yamada T., 2001, PASJ, 53, 833
Kawakatu N., Imanishi M., Nagao T., 2007, ApJ, 661, 660
King A. R., Pringle J. E., 2007, MNRAS, 377, L25
King A. R., Pringle J. E., Hofmann J. A., 2008, MNRAS, 385, 1621
Komossa S., 2008, Rev. Mex. Astron. Astrofis. Ser. Conf., 32, 86
Komossa S., Xu D., 2007, ApJ, 667, L33
Kormendy J., Kennicutt R. C., Jr, 2004, ARA&A, 42, 603
Kormendy J., Bender R., Cornell M. E., 2011, Nat, 469, 374
Laurikainen E., Salo H., Buta R., Knapen J. H., 2007, MNRAS, 381, 401
Maciejewski W., 2004a, MNRAS, 354, 883
Maciejewski W., 2004b, MNRAS, 354, 892
Maiolino R., Rieke G. H., 1995, ApJ, 454, 95
Malkan M. A., Gorjian V., Tam R., 1998, ApJS, 117, 25
Marconi A., Axon D. J., Maiolino R., Nagao T., Pastorini G., Pietrini P., Robinson A., Torricelli G., 2008, ApJ, 678, 693
Marinova I., Jogee S., 2007, ApJ, 659, 1176
Márquez I. et al., 2004, A&A, 416, 475
Martini P., Regan M. W., Mulchaey J. S., Pogge R. W., 2003, ApJ, 589, 774
Masters K. L. et al., 2010, MNRAS, 404, 792
Mathur S., 2000, MNRAS, 314, L17
Mathur S., Grupe D., 2005a, A&A, 432, 463
Mathur S., Grupe D., 2005b, ApJ, 633, 688
Mathur S., Kuraszkiewicz J., Czerny B., 2001, Nat, 6, 321
Mathur S., Fields D., Peterson B. M., Grupe D., 2011, preprint (astro-ph/1102.0537)
Miniutti G., Panessa F., de Rosa A., Fabian A. C., Malizia A., Molina M., Miller J. M., Vaughan S., 2009, MNRAS, 398, 255
Nelson C. H., 2000, ApJ, 544, L91
Nowak N., Thomas J., Erwin P., Saglia R. P., Bender R., Davies R. I., 2010, MNRAS, 403, 646
Oesch P. A. et al., 2010, ApJ, 714, L47
Ohta K., Aoki K., Kawaguchi T., Kiuchi G., 2007, ApJS, 169, 1
Osterbrock D. E., Martel A., 1993, ApJ, 414, 552
Parry O. H., Eke V. R., Frenk C. S., 2009, MNRAS, 396, 1972
Peng C. Y., 2007, ApJ, 671, 1098
Peng C. Y., Ho L. C., Impey C. D., Rix H., 2010, AJ, 139, 2097
Ponti G. et al., 2010, MNRAS, 406, 2591

Ramos Almeida C. et al., 2009, ApJ, 702, 1127
Ryan C. J., De Robertis M. M., Virani S., Laor A., Dawson P. C., 2007, ApJ, 654, 799
Sakamoto K., Okumura S. K., Ishizuki S., Scoville N. Z., 1999, ApJ, 525, 691
Sani E., Lutz D., Risaliti G., Netzer H., Gallo L. C., Trakhtenbrot B., Sturm E., Boller T., 2010, MNRAS, 403, 1246
Sani E., Marconi A., Hunt L. K., Risaliti G., 2011, MNRAS, 413, 1479
Sheth K., Regan M. W., Scoville N. Z., Strubbe L. E., 2003, ApJ, 592, L13
Sheth K., Vogel S. N., Regan M. W., Thornley M. D., Teuben P. J., 2005, ApJ, 632, 217
Sheth K. et al., 2008, ApJ, 675, 1141
Shlosman I., Peletier R. F., Knapen J. H., 2000, ApJ, 535, L83
Tran H. D., 2010, ApJ, 711, 1174
van den Bergh S., Cohen J. G., Hogg D. W., Blandford R., 2000, AJ, 120, 2190
Véron-Cetty M., Véron P., 2001, A&A, 374, 92
Véron-Cetty M., Véron P., 2010, A&A, 518, A10
Véron-Cetty M., Véron P., Gonçalves A. C., 2001, A&A, 372, 730
Volonteri M., 2010, A&AR, 18, 279
Volonteri M., Madau P., Quataert E., Rees M. J., 2005, ApJ, 620, 69
Wang J., Zhang E., 2007, ApJ, 660, 1072
Weinzirl T., Jogee S., Khochfar S., Burkert A., Kormendy J., 2009, ApJ, 696, 411
Williams R. J., Pogge R. W., Mathur S., 2002, AJ, 124, 3042
Zhang E., Wang J., 2006, ApJ, 653, 137
Zhou H., Wang T., Yuan W., Lu H., Dong X., Wang J., Lu Y., 2006, ApJS, 166, 128
Zhu L., Zhang S. N., Tang S., 2009, ApJ, 700, 1173

## APPENDIX A: SÉRSIC LIGHT PROFILE

The Sérsic power-law intensity profile is frequently used in the study of galaxy morphology. It has the following functional form (e.g. Caon, Capaccioli & D'Onofrio 1993; Peng et al. 2010):

$$I(r) = I_{\rm e} \exp\left[-\kappa\left(\left(\frac{r}{r_{\rm e}}\right)^{1/n} - 1\right)\right], \quad \text{(A1)}$$

where $I_{\rm e}$ is the surface brightness at the effective radius $r_{\rm e}$. The parameter $r_{\rm e}$ is known as the effective, or half-light, radius, defined such that half of the total flux lies within $r_{\rm e}$. The parameter $n$ is the Sérsic index: with $n = 4$ the profile is the de Vaucouleurs profile typical of elliptical galaxies, $n = 0.5$ gives a Gaussian and $n = 1$ is the exponential profile typical of discs. Finally, the parameter $\kappa$ is in fact coupled to $n$ and is not a free parameter.

The exponential disc profile is more frequently described by the compact form

$$I(r) = I_0 \exp\left(-\frac{r}{r_{\rm s}}\right), \quad \text{(A2)}$$

where $I_0$ is the central surface brightness, $I_0 = I_{\rm e}e^{\kappa}$, and $r_{\rm s}$ the scale radius given by $r_{\rm e} = 1.678 r_{\rm s}$, or more generally by $r_{\rm e} = \kappa^n r_{\rm s}$.

### A1 Sérsic luminosity ratios

The bulge-to-disc ($B/D$) and bulge-to-total ($B/T$) luminosity ratios are relevant quantities for the study of galaxy morphology. These ratios tend to decrease from early- to late-type spirals (e.g. Masters et al. 2010). The $B/D$ ratio, where the disc is described by an exponential profile, can be expressed analytically as

$$\frac{B}{D} = \frac{n_{\rm b}\Gamma(2n_{\rm b})e^{\kappa}}{\kappa^{2n_{\rm b}}}\left(\frac{q_{\rm b}R_{\rm b}^2}{q_{\rm d}R_{\rm d}^2}\right)\left(\frac{I_{\rm e}}{I_0}\right), \quad \text{(A3)}$$

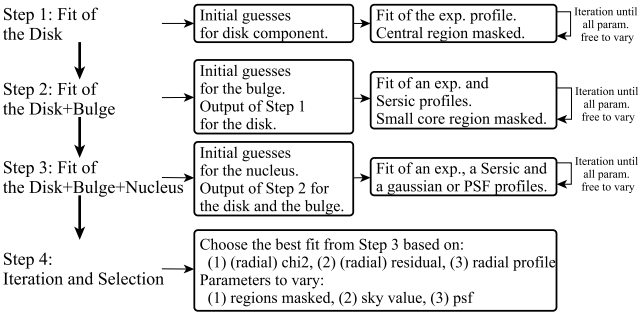


**Figure B1.** Our iterative fitting procedure.

and the $B/T$ as

$$\frac{B}{T} = \frac{n_{\rm b}\Gamma(2n_{\rm b})e^{\kappa}/\kappa^{2n_{\rm b}}q_{\rm b}R_{\rm b}^2 I_{\rm e}}{n_{\rm b}\Gamma(2n_{\rm b})e^{\kappa}/\kappa^{2n_{\rm b}}q_{\rm b}R_{\rm b}^2 I_{\rm e} + q_{\rm d}R_{\rm d}^2 I_0}, \quad \text{(A4)}$$

where the subscripts 'b' and 'd' refer to the bulge and the disc, respectively. $I_{\rm e}$ is the effective surface brightness of the bulge and $I_0$ is the central surface brightness of the disc, $R_{\rm b}$ is the effective radius of the bulge, $R_{\rm d}$ the scale radius of the disc and $q_{\rm b}$, $q_{\rm d}$ are the axis ratios of the respective profiles. To calculate the parameter $\kappa$, we use the analytic expansion equation (18) from Ciotti & Bertin (1999) valid for $n > 0.36$.

## APPENDIX B: FIT PROCEDURE

To accomplish the bulge–disc decomposition, we use the two-dimensional profile fitting algorithm GALFIT (Peng et al. 2010), which allows, by minimizing the $\chi^2$ value, to model the light profiles using e.g. Sérsic profiles.

Since we fit *HST* images, we generate the PSFs with the TINYTIM[6] code for the WFPC2 camera as well as the *F606W* filter. For each image, we create a PSF referenced to the galaxy centre with a uniform weight along the wavelength range.

Initial parameters are estimated from visual inspection of the images (positions, position angle, ellipticities, radii, etc.). Nevertheless, our iterative fit procedure, as described hereafter, ensure that the choice of initial estimates do not influence the final results.

Our procedure can be divided in four steps as summarized in Fig. B1. For each step we create appropriated masks to remove regions from the fits.

(1) We start by fitting only the disc of the galaxies using an exponential profile and masking the central region.

(2) Once a reasonable model is obtained, we fit an additional Sérsic component to model the bulge. Our initial estimate of the Sérsic index is $n_{\rm b} = 2$ (i.e. the index threshold between pseudo- and classical bulges), while the other parameter initial estimates are based upon visual inspection. When fitting, we first keep the outputs of our step 1 fixed in the fit and then free to vary (together with the Sérsic profile parameters). During this step we mask only the core of the galaxies (5 to 10 pixels radius) to avoid possible influence of the central nucleus or AGN source.

(3) We then fit an additional Gaussian (with initial FWHM of 2.5 pixels) to model the AGN and iterate, if necessary, until all parameters are free to vary. As a non-negligible fraction of the images presents a saturated core with charges leakage along the

[6] http://www.stsci.edu/software/tinytim/

columns (34 per cent in total, 50 per cent in the NLS1 and 26 per cent in the BLS1 samples), we mask carefully these pixels. We also verify the resulting FWHM of the Gaussian and its axial ratio. An additional motivation to use a Gaussian instead of a PSF is to model any nuclear star cluster which, if not accounted for in the fit, will artificially increase the bulge Sérsic index.

During these three steps, we judge the quality of the fit based on the residual images, the $\chi^2$ values and the parameters values (ensuring that they are physically meaningful: the magnitude of the components have to be greater than the sky level, the Sérsic index value should be acceptable, in particular $n_b < 8$, and the physical radii $R_b$ and $R_d$ should be reasonable).

(4) At the end of the third step, we additionally look at the radial profiles of the model, its components and the original image. These plots together with the radial residual and the radial $\chi^2_\nu$ enable us to diagnostic possible problems and identify influences of non-fitted structures. Upon examination of these plots and the image residuals, we decide whether it is necessary to mask relevant structures such as rings or spirals. We refine the masks and the fits until the radial profile of the model does not appear to be influenced by these structures but do translate correctly the bulge and the disc components.

While the GALFIT outputs provide errors, those are purely statistical and are insignificant compared to systematic errors. In the

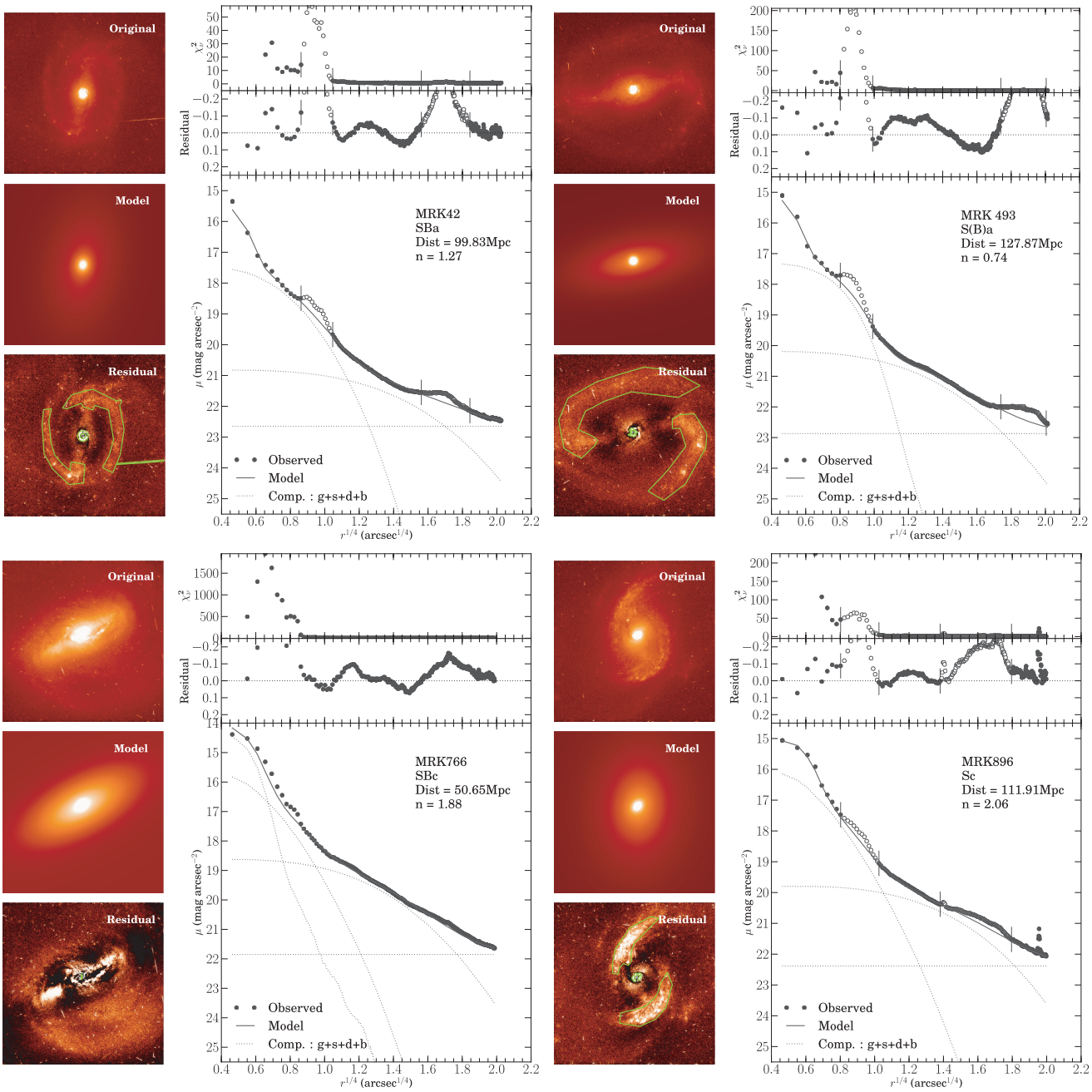


**Figure B2.** Bulge–disc decomposition illustration from the NLS1 sample. The radial ranges of the mask are indicated by open symbols and straight lines in the radial profiles. The upper plot gives the radial distribution of the reduced $\chi^2$, the middle plot is the magnitude difference $\Delta\mu$ between the original and the model images and the bottom plot presents the observed (dots), the total model (solid line), the modelled bulge and the modelled disc (dashed) light distributions. The radius is given in $r^{1/4}$ to emphasize the central region.

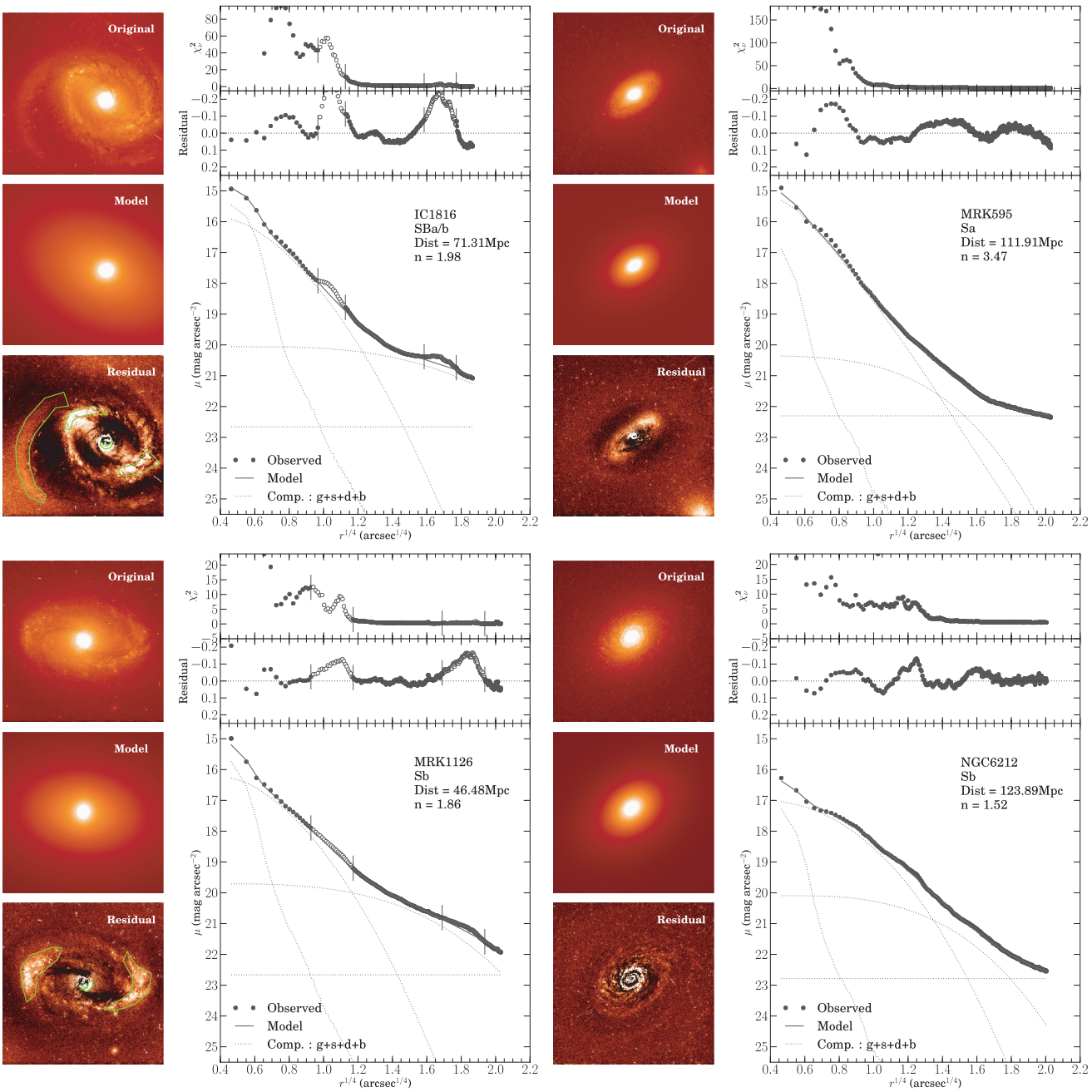


**Figure B3.** Bulge–disc decomposition illustration from the BLS1 sample. The radial ranges of the mask are indicated by open symbols and straight lines in the radial profiles. The upper plot gives the radial distribution of the reduced $\chi^2$, the middle plot is the magnitude difference $\Delta\mu$ between the original and the model images and the bottom plot presents the observed (dots), the total model (solid line), the modelled bulge and the modelled disc (dashed) light distributions. The radius is given in $r^{1/4}$ to emphasize the central region.

following sections, we discuss the robustness of our fits to different parameters: the treatment of additional structures (deviation from idealized profiles), the unprecise knowledge of the background level, the core saturation and the PSF. Those parameters give indirect information on the systematic errors. Finally, we give in Figs B2 and B3 eight examples of our fits where we indicate by open symbols the radial ranges entirely or partially masked. The radial residual and the radial $\chi^2_\nu$, given in the upper panels, also provide indirect information on the fit errors.

### B1 Choice of fitting range: treatment of additional structures

As already mentioned, any nucleus is accounted for in the fits by the use of a small Gaussian profile. The alternative consists of removing the nucleus from the fit by masking it. Nevertheless, with such a procedure, the bulge–disc decomposition is sensitive to the quality of the mask of the nucleus and can also be affected by the reduced number of constraints, i.e. the bulge can be underconstrained if the mask is too large. Despite these considerations, we try the alternative and mask systematically the central region of the images. We use a

default circular mask with 10 pixels radius, adjusting it only in a few cases (4/28) to have a minimum radius of five times the standard deviation $\sigma$ of the Gaussian component (2/4) or to keep a reasonable number of constraints for the bulges (2/4). The median Sérsic index difference between the fits with nucleus masked and the fits with the nucleus included is reasonably small: 0.22 and 0.29 for the NLS1 and BLS1 sample, respectively. This test shows that to mask the nucleus instead of fitting it by a Gaussian component biases slightly the Sérsic indices to higher values. Nevertheless, except for a few cases (3/28 with $\Delta n_\mathrm{b} > 2$ and 2/28 with $2 > \Delta n_\mathrm{b} > 1$), the increase remains small, acknowledging the robustness of the fits.

As our samples are made of high-resolution *HST* data, they also present many structural details. The effect of deviations of surface brightness such as rings, bars or spirals is considered in the last step of our fitting procedure (step 4). Upon examination of the radial profiles and the residual image, we identify, if any, potential additional structures and manually create appropriate two-dimensional masks. We then refit our model and iteratively adjust the mask according to the radial profile and residual image. We recognize that this practice is subjective but none the less we believe it to be necessary. Indeed, modelling structural details – such as inner rings – is a complex task, and the fit of any additional component requires more constraints, which cannot be provided by our single snapshot *HST* images (indeed the current bulge–disc models already give $\chi^2_\nu \sim 1$ for most of the fits). The alternative practice of not masking these structures could lead to wrong results. For example, in the case of MRK 42, presented in Fig. B2, we first do not mask the inner ring and obtain a compact bulge with $n_\mathrm{b} \sim 0.7$ (in our step 3), while after masking the structure, we obtain a more reasonable Sérsic index $n_\mathrm{b} \sim 1.27$ (in our step 4), which – according to the radial profile in Fig. B2 – is a much more accurate model of the bulge. Finally, our iterative process ensures that the regions we mask are physical additional structures in the galaxies.

### B2 Background level

Given that the background may be coupled to the disc profile, an important aspect of bulge–disc decomposition is to correctly fix the sky level. Since no precise sky measurements are available for our *HST* images and that the galaxies filled most of the field of view, we have to fit the background level together with the other components and minimize the coupling with the disc profile. Therefore, we take a particular care to any additional light profiles in the images such as stars, satellite galaxies or remaining large cosmic rays. These are carefully masked so to minimize their influence on the sky level. Despite this particular attention, we fix the sky level in two cases – MRK 279 and MRK 609, both part of the BLS1 sample – at the value obtained in our step 1 (i.e. fit of the disc and the background only). If the sky is not fixed, the resulting parameters are not physical: in the case of MRK 279 the background becomes negative and the radius of the disc excessively large; in the case of MRK 609 the sky becomes extremely large and the disc and the bulge shrink (with $n_\mathrm{b} < 0.5$).

## APPENDIX C: RELIABILITY OF THE BULGE–DISC DECOMPOSITION

We analyse here possible effects influencing our fit results: the core saturation in the images and the choice of PSF.

As already mentioned, a non-negligible fraction of the images presents saturated core with charges leakage: 50 per cent in the NLS1 sample and 26 per cent in the BLS1 sample. To minimize any effect on our fits, we mask carefully the saturated pixels and the pixels affected by charges leakage. Looking at the Sérsic indices, we find that galaxies with saturated core have a mean Sérsic index $\langle n_\mathrm{b} \rangle = 2.27$ and galaxies without saturated core have $\langle n_\mathrm{b} \rangle = 2.06$. Therefore, if the saturation still affect our images, it would tend to increase the Sérsic index. As our NLS1 sample is more affected by saturation than our BLS1 sample, it would tend to increase the mean Sérsic index of NLS1s. Consequently, any remaining effect of the saturation cannot account for the difference between NLS1 and BLS1 host bulge Sérsic indices but would tend to decrease it.

We test the dependence of our fit to the PSF used for convolution by refitting our NLS1 sample with different PSFs. The PSFs for this test are also generated with TINYTIM but, instead of using a uniform weight along the wavelength range, they are produced at the central monowavelength of the filter *F606W*. The difference in Sérsic index ranges from 0 to 0.01 except for one object where it is 0.06. Therefore, we conclude that the PSFs are not critical in our fits and that our choice of using a uniform weight along the wavelength range to create the PSFs with TINYTIM is acceptable.

This paper has been typeset from a TEX/LATEX file prepared by the author.